Review Article

Near-Field Thermophotovoltaic Energy Conversion: Progress and Opportunities

Rohith Mittapally,[1] Ayan Majumder,[1] Pramod Reddy,[1,2,3,*] and Edgar Meyhofer[1,4,†]

[1]*Department of Mechanical Engineering, University of Michigan, Ann Arbor, Michigan 48109, USA*

[2]*Department of Electrical Engineering and Computer Science, University of Michigan, Ann Arbor, Michigan 48109, USA*

[3]*Department of Materials Science and Engineering, University of Michigan, Ann Arbor, Michigan 48109, USA*

[4]*Department of Biomedical Engineering, University of Michigan, Ann Arbor, Michigan 48109, USA*

Direct conversion of heat to electricity via solid-state approaches is a rapidly advancing area of research owing to its prospective use in recovering waste heat and in energy storage and utilization. In particular, thermophotovoltaic (TPV) approaches that take advantage of near-field (NF) evanescent modes are receiving increased attention due to their potential for increased power output. This review examines the latest progress in theoretical and experimental explorations of near-field thermophotovoltaic (NF TPV) systems. We begin by introducing thermal radiation, its use in TPV systems, and how these systems have developed over time. Next, we describe the fundamentals of NF radiative heat transfer, as well as the operating principles and models used to evaluate NF TPV systems. We discuss theoretical studies, based on fluctuational electrodynamics, that have predicted large enhancements in radiative energy transfer and consequently large electrical power outputs in NF TPV systems. Subsequently, we summarize recent advances in the experimental exploration of NF TPV systems and describe how researchers have recently developed unique experimental platforms to explore the principles of NF TPVs and have achieved significant enhancements in power output at reasonable conversion efficiencies. Additionally, we discuss related thermoradiative and thermophotonic energy conversion systems that provide interesting new avenues for photonic energy conversion. These systems, while theoretically promising, still await experimental validation in realistic material systems. Finally, we present remarks on the future potential of NF TPV systems and opportunities for improving NF TPV performance, and discuss the challenges that must be overcome to achieve large-scale NF TPV devices.

I. INTRODUCTION

Heat engines that convert heat to electricity play a key role in energizing our everyday lives. In contrast to power conversion cycles based on traditional working fluids, solid-state approaches for heat-to-electricity conversion, such as thermoelectric [1], thermophotovoltaic [2], or thermionic energy conversion [3], enable modular, noiseless energy conversion with no moving parts. Among these, thermoelectric energy conversion has received extensive attention resulting in significant advances in recent years [4–6]. Thermophotovoltaics (TPVs) represent an alternative, solid-state energy-conversion approach that transforms emitted thermal radiation directly into electricity and offers a promising avenue for harvesting waste heat, especially at elevated temperatures, where thermoelectric materials are unstable [7]. For TPV systems to

be of practical importance in energy conversion applications, a broad range of performance improvements are actively being sought. Here, we focus on the description of a class of TPV devices, called near-field (NF) TPV systems, that hold promise—based on recent theoretical and experimental work—for large enhancements in electrical power output by taking advantage of NF radiative energy transfer, which in turn is based on the tunneling of photons across the nanoscale gap of a TPV device.

Among all modes of heat transfer, radiative energy transfer is unique as it does not require a material medium. In fact, radiative heat transfer (RHT) plays a central role in numerous phenomena including global warming, photovoltaic energy conversion, and radiative cooling. RHT, when bodies are separated by nanometric gaps, is called near-field radiative heat transfer (NF RHT). Currently, it is generally assumed that NF RHT has potential for applications in TPVs [8–12], photonic refrigeration [13,14], thermal management [15–18], scanning thermal microscopy [19–21], and heat-assisted magnetic recording [22].

*pramodr@umich.edu
†meyhofer@umich.edu

This review article is organized into the following sections: In the first section, we introduce the concept of NF RHT and TPV systems. Specifically, we discuss the fundamental differences between far-field radiative heat transfer (FF RHT) and NF RHT and discuss how RHT at the nanoscale can be modeled via the framework of fluctuational electrodynamics (FED) to quantitatively describe NF RHT. Further, past developments of TPV systems in the far field are briefly reviewed to provide a useful comparison to NF TPV systems. In the second section, we describe the operating principles of NF TPV systems along with a relatively simple model that captures the essential physics of NF TPV systems and conclude with a brief review of theoretical developments in understanding and improving the performance of NF TPV systems. In the third section, we analyze several experimental platforms that have been developed recently and have successfully overcome the numerous experimental challenges in exploring NF TPV conversion. In the fourth section, we discuss related photonic energy conversion techniques, such as thermoradiative (TR) and thermophotonic (TPX) power generation. Finally, we end with a discussion on the future opportunities for realizing large-scale NF TPV systems as well as improving their performance.

A. Near-field thermal radiation and thermophotovoltaics

A TPV system consists of a hot body that is typically at temperatures much higher than room temperature (300 K) and a photovoltaic cell (PV) nominally at room temperature (see Fig. 1). The hot body emits electromagnetic radiation whose FF spectral characteristics are described by Planck's theory of thermal radiation [23] and has an emission rate that is constrained by the blackbody limit. This radiation, when incident on the PV cell, excites electron-hole pairs that are separated due to a built-in electric field (e.g., in the depletion region of a p-n junction or due to a Schottky barrier) of the PV cell to generate an electric current. Only photons that are above the band gap (ABG) of the PV cell excite these charge carriers and contribute to power output, while the sub-band-gap (SBG) photons are largely absorbed in the cold PV cell and are lost as heat. Two parameters that characterize the performance of a TPV system are (i) radiative conversion efficiency (RCE), defined as the ratio of the electrical power output to the total RHT; and (ii) power density (P_{PV}), which is the electrical power output per unit area of the emitter or PV cell. Since TPV energy conversion is a coupled phenomenon involving transport of photons and charge carriers, the overall efficiency of a TPV system is affected by the
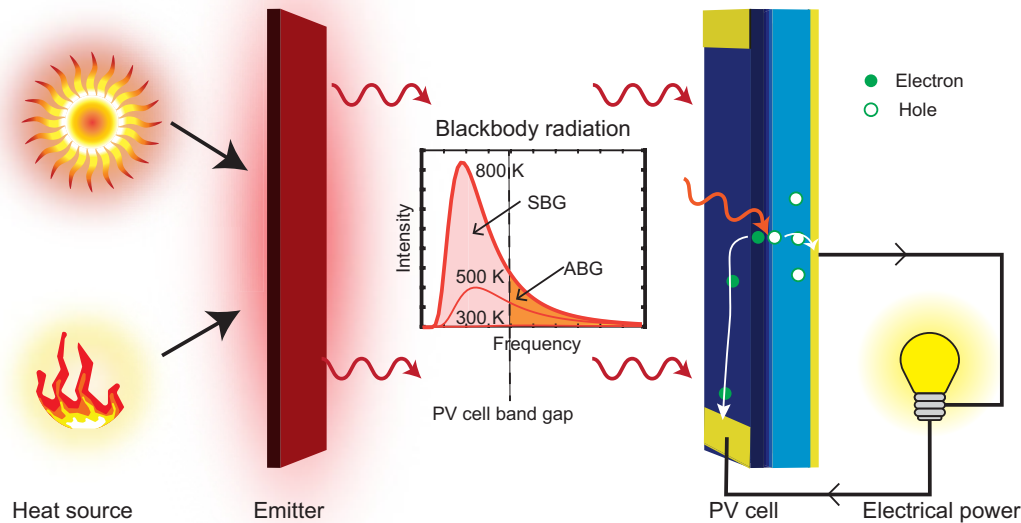

FIG. 1. Schematic of a thermophotovoltaic system (TPV) with energy sources that heat an emitter to a high temperature, and a photovoltaic (PV) cell that converts the thermal radiation from the emitter to electric power. This hot emitter radiates electromagnetic radiation whose energy distribution is described by Planck's law. The plot shows the typical spectral intensity profiles of a blackbody at different temperatures. For a PV cell with a given band gap, the orange above-band-gap (ABG) region contributes to electricity generation, while the pink sub-band-gap (SBG) region is limited to radiative heat transfer. Absorbed ABG photons create electron-hole pairs, where ideally the minority carriers are swept across the p-n junction, resulting in power generation in the external circuit. Absorbed ABG photons create electron-hole pairs, which are separated by a built-in electric field (e.g., in the depletion region of a p-n junction) to generate an electric current.

TABLE I. Summary of results from computational studies of NF TPV energy conversion. The table reports the emitter materials and their highest temperatures, PV cell materials (which were at room temperature), power density, efficiency at a representative emitter temperature, and gap size.

Publication year	Emitter material [highest temperature ($^\circ$C)]	PV cell	Power density (W/m^2)	RCE [Carnot limit] (%)	Gap (nm)
2006 [24]	Tungsten [1727]	GaSb	10×10^5	27 [85]	10
2008 [25]	Tungsten [1727]	(In, Ga)Sb	30×10^5	20 [85]	10
2015 [26]	Tungsten [527]	GaSb	840	39 [63]	10
2015 [27]	Ge [727]	GaSb	...	38.7 [70]	100
2017 [28]	ITO [627]	InAs	1.1×10^5	$\sim$40 [67]	10
2019 [29]	Graphite [727]	InAs	6.7×10^4	18 [70]	100
2020 [30]	ITO [1000]	InAs	8×10^5	50 [76]	10

spectral utilization of emitted photons, internal quantum efficiency (the number of *e-h* pairs generated per photon absorbed), and the charge carrier separation efficiency. We note that the upper bound for the efficiency of NF TPV devices (which are heat engines) operating between a hot body at temperature T_h and a cold body at temperature T_c is given the Carnot limit $\eta_c = (1 - T_c/T_h)100\%$. To compare various computational and experimental NF TPV systems discussed in this review, we also include the Carnot limit in Tables I and II. In the following subsections, we first examine the unique properties of RHT at the nanoscale. Subsequently, we present a brief overview of the experimental advances in characterizing NF RHT and FF TPV systems

1. Near-field radiative heat transfer

Radiation emitted by a hot body into its surroundings can be related to microscopic thermal oscillations of charges inside a body. First successful descriptions of far-field thermal radiation involved the concept of a macroscopic blackbody [23], which to an excellent approximation is represented by an isothermal cavity with a small hole. Any ray that enters the cavity undergoes multiple

reflections and absorptions, eventually getting completely absorbed before being able to exit the cavity. The spectral emissive power ($E_\omega(\omega, T)$) of a blackbody, i.e., radiation emanating from such a cavity, is given by [32]

$$E_\omega(\omega, T) = \left(\frac{\omega}{2\pi c}\right)^2 \frac{\hbar\omega}{exp\,(\hbar\omega/k_B T) - 1}, \quad (1)$$

where ω is the angular frequency, c is the speed of light, $\hbar$ is the reduced Planck's constant, T is the temperature of the body, and k_B is the Boltzmann constant. This distribution has, for a prescribed temperature, a maximum, which is defined by Wien's law as $\lambda_{max}T = 2898\ \mu$mK, where λ_{max} is the wavelength at which the spectral intensity peaks for a given temperature T, as illustrated in Fig. 1. At room temperature, this peak wavelength, called the Wien's wavelength (λ_{Wien}), is around 10 μm. Integrating the blackbody emissive power over all the frequencies results in the Stefan-Boltzmann law [23], where the radiative flux per unit area is σT^4, with σ being the Stefan-Boltzmann constant. The RHT flux between two objects at different temperatures T_1, T_2 is constrained by the blackbody limit derived from the Stefan-Boltzmann law and is given by $\sigma(T_2^4 - T_1^4)$.

TABLE II. Summary of NF TPV experiments. The table reports the emitter materials along with their temperatures, PV cell materials (which were at room temperature unless otherwise indicated), highest measured power density, efficiency at the relevant temperature, and smallest gap size achieved.

Publication year	Emitter material [highest temperature ($^\circ$C)]	PV cell	Power density (W/m^2) [enhancement]	RCE [Carnot limit] (%)	Smallest gap (nm)
2018 [8]	Doped silicon [382]	(In, As)Sb	6 [40-fold]	$\sim$0.02 [54]	60
2019 [9]	Silicon [800]	(In, Ga)As	120 [10-fold]	0.98 [72]	140
2020 [10]	Tungsten [607]	Ge	0.01 [11-fold]	<0.01 [66]	100
2021 [11]	Graphite sphere [460]	InSb[a]	7×10^3 [4.6-fold]	14 [90]	$\sim$100
2021 [12]	Doped silicon [1000]	(In, Ga)As	5×10^3 [4–8-fold]	6.8 [76]	100
2021 [31]	Silicon [919]	(In, Ga)As	1.92×10^3	0.7[b] [75]	140

[a]PV cell at 77K
[b]Inoue *et al*. [31] report a system-level efficiency rather than RCE.

In his seminal work [32], Planck acknowledged the limitations of his approach, which cannot explain the radiative heat transfer rate when the characteristic gaps [33–36] or the dimensions of the involved objects [37,38] are comparable to or much less than λ_{Wien}. For example, when the gap between two macroscopic planar surfaces is less than λ_{Wien}, the objects are said to be in the near field of each other. Under such conditions, Planck's theory, which was developed for objects that are much farther away than λ_{Wien} (i.e., objects in the far field of each other), cannot be applied. At these smaller gaps, the ray picture of light is no longer valid in describing NF RHT, where evanescent and surface modes lead to significant enhancements in RHT. To explore this regime, Rytov *et al.* [39] and Polder and Van Hove [40], developed the framework of FED, where thermal radiation and heat transfer between objects is related to thermal fluctuations of charges in the material. The correlation function for these thermally induced fluctuation electric currents (J), which forms a key input to the FED framework, is given by the fluctuation-dissipation theorem [41,42],

$$
\langle J_l(r,\omega)\, J_m^*(r,\omega) \rangle = \frac{4\omega}{\pi} \varepsilon_0 \varepsilon'' \Theta(\omega, T) \delta_{lm} \delta
$$
$$
\times\, (r - r')\delta(\omega - \omega'), \qquad (2)
$$

where $\Theta(\omega, T) = \hbar\omega/(e^{((\hbar\omega)/k_B T)} - 1)$ is the mean energy of a harmonic oscillator, $\hbar$ is the reduced Planck constant, T is the absolute temperature, and ε'' is the imaginary component of the dielectric function ε_0. The Kronecker delta δ_{lm} indicates no cross-coupling between currents in orthogonal directions represented by the subscripts l and m, while the Dirac delta $\delta(r - r')$ reflects the assumption of locality, excluding spatial dispersions in the media.

First experiments to quantify NF RHT were performed by Hargreaves [43] in 1969, where the RHT between metallic parallel plates was measured down to gaps of a few micrometers, and by Domoto *et al.* [44] in 1970 between metallic plates at liquid-helium temperature. While these studies indicated enhanced RHT at microscale gaps, the true potential of NF RHT was only realized in early 2000s when several experiments [33–36,45,46] were performed in sphere-plate or tip-plate configurations, owing to their simplicity in comparison with the extended plate-plate configuration, and showed RHT enhancements at nanometric distances. A limitation of this approach is that only a small region near the periphery of the sphere or the tip and close to the plate is effectively contributing to the NF enhancements. Further, the sphere-plate configuration is less well suited to quantitative comparisons with the predictions of FED and researchers typically had to resort to the use of proximity approximations to discretize the curved surfaces as planes. Clear demonstrations of the enhancement in RHT via measurements in the plate-plate configuration down to gaps as small as tens of

nanometers became possible only in the last decade, aided by the development of microdevices, precise calorimetric techniques, and precise alignment between the devices [17,47–55]. These experiments enabled both the probing of NF RHT between planar dielectric and metallic surfaces and quantitative comparisons with the predictions of FED, confirming its validity for modeling NF RHT. Detailed and comprehensive descriptions of these advances can be found in recent reviews [56–58].

2. Thermophotovoltaic systems

The history of TPV power generation dates back to the 1960s, when a TPV system [59] was first conceptualized as an alternative to thermoelectric and thermionic energy conversion devices. The energy crisis in the 1970s led to interest in renewable energy technologies including TPV technologies [60]. Although research in TPV systems slowed down in the 1980s, some researchers continued to work on developing low-band-gap cells using (In, Ga)As [61] that were better suited for TPV devices. Since the early 1990s, research motivated by specific mission-driven applications of NASA and DARPA has enabled development of a variety of TPV systems, including radio isotope–powered TPV devices [62], fossil fuel–powered TPV devices based on GaSb cells [63], and TPV devices for waste heat conversion [64].

Several research efforts were aimed at improving the overall efficiency of TPV systems by engineering the spectral characteristics of thermal radiation either through an intermediate spectral control device or by structuring the emitters of the TPV devices. In 2004, Wernsman *et al.* [64] reported 23.6% thermal-to-electricity conversion using a SiC emitter heated to 1039 °C and an (In, Ga)As-based monolithic interconnected module. This record efficiency was recently improved upon by employing a thin-film (In, Ga)As cell featuring a back-surface reflector (BSR) and a graphite emitter at 1027 °C [65], leading to an efficiency of 29.1%. Further, Fan *et al.* [66] recently developed air-bridge thin-film (In, Ga)As cells such that the sub-band-gap photons are reflected due to total internal reflection. They reported an efficiency of >30% using a SiC emitter at 1180 °C. More recently, LaPotin *et al.* [67] pursued even higher temperatures along with high-performance multijunction PV architectures and reported a power density of 24×10^3 W/m^2 when the emitter was at 2127 °C and a measured efficiency of 41.1%. A more detailed discussion of FF TPV systems is found in recent review articles [2,68,69]. Tervo *et al.* [70] fabricated large-area single-junction (In, Ga)As cells and reported a power density of 37.8×10^3 W/m^2 at an efficiency of 38.8% using a graphite emitter heated to 1850 °C. Further, López *et al.* [71] improved the standard experimental approach to increase the view factor, thus obtaining relatively large power densities of 43×10^3 W/m^2 at an efficiency of

26.4% when irradiated by a graphite emitter heated at 1592 °C. We note that all these TPV demonstrations rely on FF thermal radiation as the emitter and PV cell are separated by gaps much larger than the characteristic λ_{Wien}. Therefore, in all these studies the energy transfer rate from the emitter to the PV cell is below the blackbody limit. In the next section we describe how this limit can be overcome by operation in the NF. Further, we discuss some of the theoretical predictions related to NF TPV devices.

II. MODELING OF NEAR-FIELD THERMOPHOTOVOLTAIC ENERGY CONVERSION

Analysis of FF TPV systems relies on the classical theory of thermal radiation for modeling the thermal characteristics of the emitter, while the PV cell is modeled using traditional device models [69] for PV cells. Modeling of NF TPV systems requires a more sophisticated analysis based on using FED in conjunction with traditional device models of PV cells. In the following, we present one version of such a model for analyzing NF TPV systems that involves first calculating the number of photons absorbed by the PV cell and subsequently utilizing an analytical PV model to calculate the power density (P_{PV}). For detailed theoretical modeling of NF TPV systems, we also refer the readers to a recent review article [72].

A. Modeling energy transfer in NF TPV devices

Energy transfer from a hot emitter to a NF TPV device is modeled using FED. In this approach, Maxwell's equations are coupled with random current sources as given by the fluctuation-dissipation theorem [39] described in Eq. (2). The radiative energy transfer is then computed by evaluating the time-averaged Poynting fluxes [56]. In Fig. 2(a), we show a schematic of a plate-plate geometry, which is relevant to almost all NF TPV systems and features a hot body and a PV cell that are semi-infinite in the lateral directions and are separated by a macroscopic gap. Several electromagnetic modes are thermally excited in the hot body, and these reach the emitter-vacuum interface. Only modes that are incident at angles smaller than the critical angle (θ_c) at the interface can propagate in the vacuum and reach the PV cell. These modes that are supported in vacuum are termed propagating waves and contribute to far-field radiative energy transfer. In the far field, integrating the energy transfer over these propagating modes leads to the blackbody limit. Modes that have incident angles larger than the critical angle are total internally reflected (called frustrated modes) and cannot propagate in the vacuum gap. While these modes are totally reflected at the interface, they leave an evanescent tail that extends into the vacuum and exponentially decays with the distance from the surface and therefore as a function of gap size.

By reducing the gap between the devices to the nanoscale [i.e., to a distance at which the two objects are in the near field of each other, see Fig. 2(b)], evanescent modes can be coupled across the vacuum interface, leading to additional channels for energy transfer [53]. Additionally, surface polariton modes that exist in some materials—surface plasmon polaritons in metallic materials, such as Au, Ag, ITO, etc. [50,55,73,74], and surface phonon polaritons in dielectric materials, such as SiO_2, SiC, etc. [50,51,54,73]—also contribute to enhanced energy transport. These surface modes are evanescent in both the material and vacuum and exist only at the interface, but for small gap sizes they lead to enhancement in energy transfer by several orders of magnitude [75] and consequently enable large improvements in the power density of NF TPV systems [8,9,12,31,76].

The first step in modeling a NF TPV system is to calculate the current density (J_{rad}) from the PV cell. The FED solution to the photon transfer between plane parallel plates (assumed to be isothermal) and subsequent current generation can be described by a Landauer-like expression [56,77],

$$J_{\text{rad}} = q\left(\frac{1}{2\pi}\right)^2 \int_{\omega_g}^{\infty} (n(\omega, T_h, 0)$$
$$- n(\omega, T_c, V)) \int_0^{\infty} \tau(\omega, k) \, k \, dk d\omega, \qquad (3)$$

where the current generated by photons in the NF with frequency $\omega > \omega_g$ (ω_g corresponds to the band gap of the PV cell) is evaluated via the transmission probability, $\tau(\omega, k)$. The transmission probability between multilayered structures can be calculated either using transfer-matrix [9,78] or scattering-matrix [8,12,79] methods. We note that, J_{rad} has a positive contribution from the irradiated photons and a negative contribution from radiative recombination. Here, we assume 100% internal quantum efficiency, i.e., each absorbed photon is assumed to generate one *e-h* pair, q is the electron charge, k is the in-plane wave number, ω is the frequency of the photon mode, T_h is the temperature of the hot emitter, T_c is the temperature of the cold PV cell, V is the voltage bias across the PV cell, $n(\omega, T, V) = 1/(e^{((\hbar\omega - qV)/k_B T)} - 1)$ is the generalized photon occupation number, k_B is the Boltzmann constant, and $\hbar\omega$ is the photon energy.

The total RHT (Q_{RHT}) from the emitter to the PV cell can also be calculated from

$$Q_{\text{RHT}} = \left(\frac{1}{2\pi}\right)^2 \int_0^{\infty} \hbar\omega(n(\omega, T_h, 0)$$
$$- n(\omega, T_c, V)) \int_0^{\infty} \tau(\omega, k) \, k \, dk d\omega. \qquad (4)$$
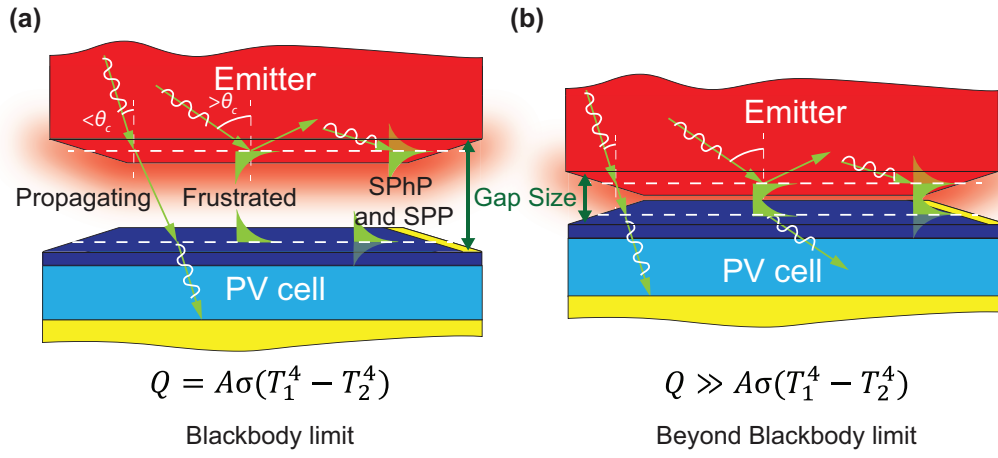
FIG. 2. Description of the role of evanescent and surface modes in NF-based TPV energy conversion. (a) Schematic description of radiative energy transfer between two isothermal, semi-infinite bodies (e.g., a hot emitter and a PV cell) separated by macroscopic gaps. Radiative energy flow occurs exclusively via propagating waves and is bounded by the blackbody limit. Surface modes, such as the frustrated, surface phonon polariton (SPhP) and surface plasmon polariton (SPP) modes, exist at the material-vacuum interface but cannot propagate in the vacuum. (b) In the near field (i.e., for nanoscale gaps), evanescent and surface modes can tunnel across the vacuum gap resulting in orders of magnitude enhancement in energy transfer between a hot emitter and a PV cell. The gap sizes in the two figures are not drawn to scale.

In the next section, we briefly review the modeling of power output extraction in the PV cell.

B. PV cell modeling

The photons transferred via near-field thermal radiation to the PV cell excite e-h pairs, which are then swept by the built-in electric field resulting in an accumulation of charges and hence a voltage [called the photovoltaic effect, see Fig. 3(a)]. When the two ends of the PV cell are directly wired together, this results in a photocurrent usually referred to as short-circuit current. Considering a detailed balance of the TPV system [80], the current density $J(V)$ of the PV cell can be expressed as [30,72]

$$J(V) = J_{rad} - J_{Auger}(V) - J_{SRH}(V), \quad (5)$$

$$J_{Auger}(V) = q(C_n n + C_p p)(np - n_i^2)t, \quad (6)$$

$$J_{SRH}(V) = q \frac{2(np - n_i^2)}{\tau(n + p + 2n_i)}, \quad (7)$$

and

$$V = V_{ext} - JR_s. \quad (8)$$

J_{rad}, as discussed above, includes the generation and the radiative recombination rates; V is the voltage bias across the PV cell; J_{Auger} and J_{SRH} are the nonradiative components corresponding to Auger recombination and Shockley-Read-Hall recombination; C_n and C_p are the Auger recombination coefficients for electron and hole, respectively; n_i is the intrinsic carrier concentration at zero

bias; n and p are the electron and hole densities, respectively, in the active layer of the device, which depend on the voltage and the doping level of the active layer; τ is the SRH lifetime; t is the thickness of the active layer of the photovoltaic cell; R_s is the series resistance; and V_{ext} is the externally applied voltage bias.

The current density when the voltage is zero is called the short-circuit current density $[J(0) = J_{rad}]$ and the voltage when there is no current flow in the circuit is called the open-circuit voltage (V_{OC}). Thus, the J-V characteristics of an illuminated PV cell resemble those shown in Fig. 3(b) and exhibit a point [marked by a star in Fig. 3(b)] called the maximum power point, where the power output from the PV cell is maximized ($P_{PV,max}$). Using the total RHT (Q_{RHT}) and the electrical power output ($P_{PV,max}$), one can estimate the RCE of NF TPV systems as RCE $= P_{PV, max}/Q_{RHT}$.

C. Computational work in modeling NF TPV performance

As described previously, NF TPV systems offer an opportunity for substantially enhancing the power output by taking advantage of photon tunneling. This promise has spurred a plethora of theoretical studies [24–28,30,81–84] that have predicted large efficiencies and power densities. For example, in a pioneering study, Pan et al. [81] showed that an enhancement of n^2 in the total spectral heat transfer from a blackbody emitter to an object or PV cell is possible in the NF, where n is the smaller of the refractive indices of the emitter and the PV cell. In another pioneering study in 2002, Whale and Cravalho [82] analyzed
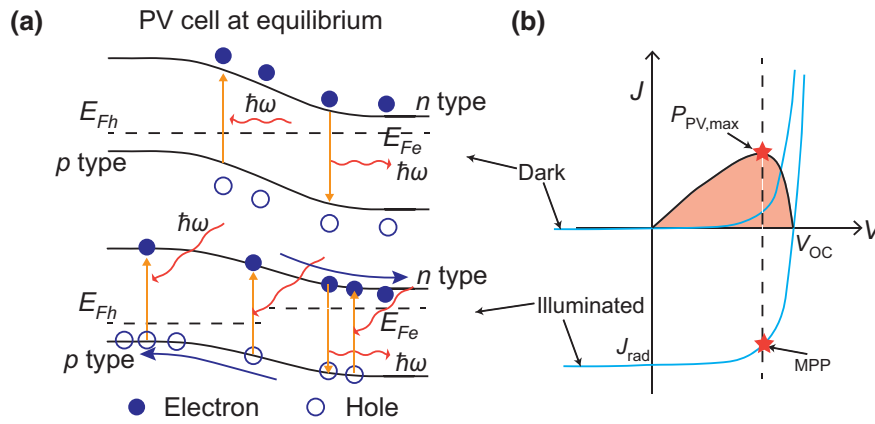
FIG. 3.   Working principle of a PV cell. (a) PV cell with a p-n junction whose band structure under equilibrium conditions is shown in the top panel. Under these conditions, e-h pairs are dynamically formed and recombine radiatively or nonradiatively. The electron and hole distributions are well characterized by a Fermi level (E_F) that is the same for both electrons and holes [i.e., $E_F = E_{Fe} = E_{Fh}$, where E_{Fe} (E_{Fh}) is the quasi-Fermi-level of electrons (holes)]. This is referred to as the "dark" condition of the PV cell and the J-V characteristics of such a state are schematically shown in (b). The bottom panel of (a) shows the band diagram of an illuminated PV cell, where excess e-h pairs are generated, resulting in a situation where $E_{Fe} \neq E_{Fh}$. In the absence of an external load, the difference in the quasi-Fermi-levels ($E_{Fe} - E_{Fh}$) corresponds to the open-circuit voltage (V_{OC}). (b) Illuminated PV cell exhibits a shift in the J-V curve towards the fourth quadrant. The number of photons absorbed indicates the short-circuit current or J_{rad}. The voltage when there is no current flow is called open-circuit voltage (V_{OC}). The power variation along the illuminated J-V curve is shown by the red shaded region and attains a maximum at the maximum power point (MPP) labeled $P_{PV,max}$.

a microscale TPV device in the NF. They predicted that power output can be enhanced by approximately 10 times over far-field operation by reducing the gap size between an emitter at 2000 K and an (In, Ga)As-based PV cell at 300 K from 10 μm to 10 nm. They pointed out that the enhanced power density is accompanied by a marginal gain in efficiency. Narayanaswamy and Chen [83] analyzed a NF TPV system using Green's function formalism for multilayered structures and considered a c-BN emitter at 1000 K facing a PV cell with a band gap of about 0.13 eV. In their work Narayanaswamy and Chen recognized the importance of enhancing the energy transfer or power output using surface phonon polaritons, as opposed to the frustrated mode–mediated enhancements described in the aforementioned study. Owing to the large density of states of surface phonon polaritons, they predicted a power absorption of 1.17×10^6 W/m^2 at a gap size of 20 nm. While they did not include a PV cell model, the work is conceptually important as it highlights the potential of polariton-mediated NF TPV systems for high power output.

Laroche *et al.* [24], in 2006, considered NF TPV systems featuring either a metal emitter (tungsten) or a quasi-monochromatic source matching the band gap of the PV cell based on GaSb; they predicted power enhancements of 20-fold and 35-fold, respectively, as compared to a black-body source in the far field. They reported that the gain in efficiency using a tungsten source is marginal, whereas utilizing a hypothetical quasimonochromatic source leads to an efficiency improvement from around 10% in the far

field to about 35% at a gap size of 10 nm. Park *et al.* [25], in 2008, analyzed a NF TPV system elucidating the spatial dependency of photocurrent generation and carrier recombination. As their calculations suggested minimal improvements in the efficiency, they proposed the use of a thin metal BSR that could improve the spectral utilization. In 2014, Bright *et al.* [84] expanded on this idea and calculated that 35% improvement in efficiency is possible by adding a mirror as compared to a semi-infinite TPV cell [Fig. 4(a)]. In 2011, Francoeur *et al.* [85] considered the impact of PV cell heating on the performance of a NF TPV system. As the near-field enhancement is broadband in nature, the heat transfer to the PV cell is also increased, imposing potential thermal management challenges on the PV cell side. For example, they computed that a cell heated from 300 to 500 K can suffer diminished efficiency from 25% to 3%. This work highlights one of the challenges in realizing practical NF TPV devices.

In 2015, Chen *et al.* [26] discussed the idea of using a PV cell made from a nonpolar semiconductor, such as Ge, to avoid heat transfer via polaritonic modes. They predicted that the efficiency of a tungsten-GaSb TPV system with the emitter at 800 K drops with reducing gap size due to higher surface phonon polariton heat transfer in GaSb. They further showed that this trend is reversed by using a Ge PV cell. Tong *et al.* [27] considered thin-film emitters and absorbers that yield a strong spectral selectivity of thermal absorption and emission and a reduction in bulk recombination losses in the thin PV cells. For a thin-film Ge emitter, supported by a perfect metal in combination
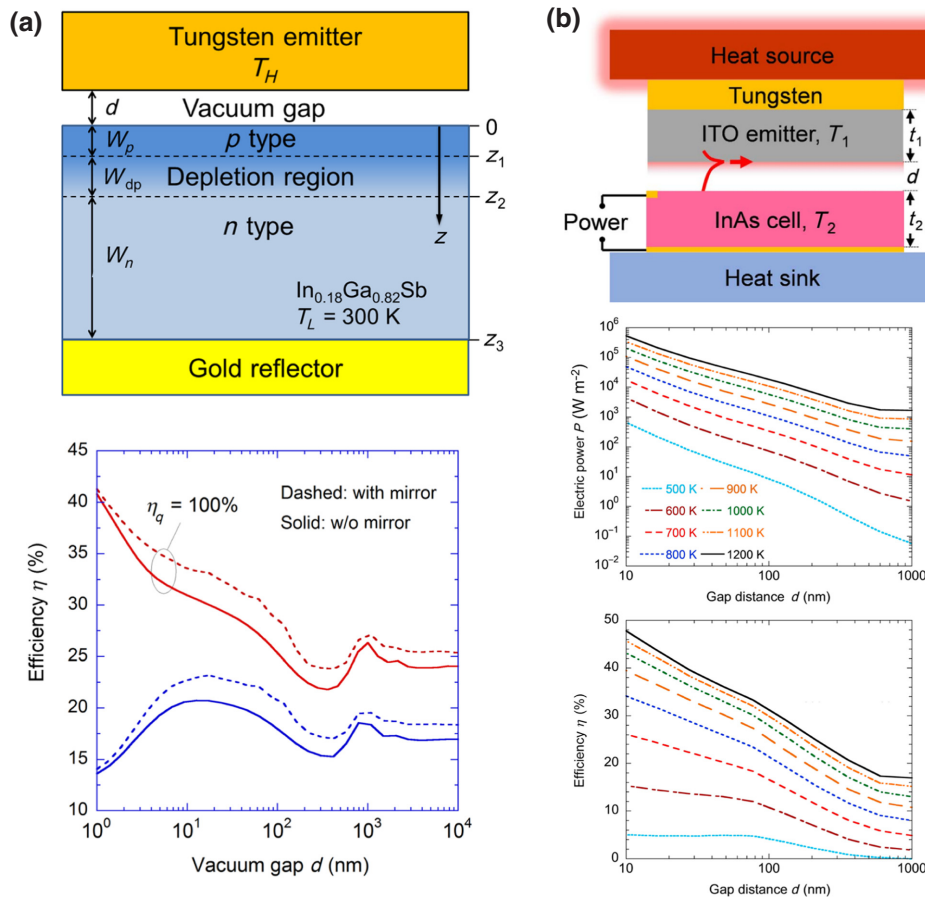
FIG. 4. Modeling of NF TPV systems. (a) NF TPV system with a tungsten emitter and a multilayered $In_{0.18}Ga_{0.82}Sb$-based PV cell with a gold back reflector (top panel) is modeled. Bottom panel presents the computed efficiency for two cases, with and without back-surface reflector (mirror), as a function of gap size when the emitter is at 2000 K. For each of these cases, calculations assume a 100% internal quantum efficiency (red) and a more realistic PV cell (blue) where nonradiative recombination is also considered. The efficiency is significantly improved for the case with a mirror (dashed lines) compared with that without a mirror (solid lines). The reduction in efficiency with reducing gap size for the blue curves is due to an increase in surface recombination at smaller gaps due to the reduced penetration depth of NF radiation. Reproduced with permission from [84]. (b) NF TPV system (top panel) with an emitter made from a thin ITO emitter supported on a tungsten base while the PV cell is an InAs-based thin-film PV cell with a back-surface reflector. The middle panel shows the power density variation as a function of gap size for emitter temperatures ranging from 500 to 1200 K. Several orders of magnitude enhancement in power output can be observed at all temperatures as the gap size is reduced. The bottom panel shows the efficiency for the same temperatures as a function of gap size. This study suggests that choosing a material that supports surface plasmon polaritons in conjunction with a low-band-gap PV cell can result in significant improvement in the efficiency at all temperatures. Reproduced with permission from [28].

with a thin PV cell, they predicted that the efficiency can be as high as 46% at an emitter temperature of 1000 K. Zhao *et al.* [28] considered an ITO-based emitter at 900 K whose plasma frequency is matched with the band gap of an InAs PV cell and predicted an efficiency of 40% at a power density of 110 kW/m^2 [Fig. 4(b)]. Papadakis *et al.* [30] considered broadening of the spectral transfer by integrating multilayer thin-film structures with different plasma frequencies instead of a narrow-band transfer (typically observed in surface plasmon polariton–mediated energy transfer) and predicted a conversion efficiency of 50% at 1300 K.

To minimize the series resistance and shadowing losses associated with electrodes on top of PV cells, Datas and Vaillon [29,86] proposed a thermionic-enhanced NF TPV system. Specifically, they considered [29] a graphite emitter at 1000 K and an InAs PV cell coated with a 1–2-nm-thick layer of H-terminated diamond film. In such a structure they suggested that "thermionic emission through the vacuum gap electrically interconnects the emitter with the front side of the photovoltaic cell and generates an additional thermionic voltage." Specifically, via computations, they showed that it is possible to generate electric power at a density of 67.3 kW/m^2 and an efficiency of

18%, which represents a 10.7-fold increase in the power and a 2.8-fold enhancement in the efficiency when compared with the NF TPV system considered in their work, which featured a series resistance of $10 \, \text{m}\Omega \, \text{cm}^2$. A recent study [87] presented first experimental steps towards the demonstration of thermionic enhanced NF TPV devices. All these theoretical studies point to the capabilities of NF TPV systems in achieving enhanced performance in direct conversion of heat to electricity. In the next section, we discuss some of the experimental advances realized in the recent past.

III. EXPERIMENTS IN NEAR-FIELD THERMOPHOTOVOLTAIC SYSTEMS

Experimental characterization of NF TPV systems has been limited due to challenges in maintaining submicron gaps while sustaining a large temperature difference between the heated emitter and a PV cell whose temperature is maintained close to room temperature. As in a FF TPV system, large temperature differentials result in higher efficiencies due to an increase in the fraction of energy of above-band-gap emission and absorption. It is also important to hold the PV cell at a temperature close to the ambient as a 0.2%–0.85% drop in efficiency is seen for every kelvin rise in temperature [88] due to an increase in dark current. In the last decade, several groups have made progress in overcoming these challenges in carefully chosen experimental platforms to perform first experimental characterizations of NF TPV systems. In this section, we discuss these recent developments.

The first experimental demonstration can be traced back to a breakthrough by DiMatteo *et al.* [76] in 2001, where a fivefold increase in photocurrent was observed when a $2.2 \times 2.2 \, \text{mm}^2$ Si heater chip was pressed against an InAs PV cell [Fig. 5(a) left panel]. The Si heater chip was microfabricated with 1-μm-tall SiO_2 spacers and two

resistors for independently heating the device and measuring the temperature. The gap was varied by pressing this chip against the PV cell using a spring-loaded quartz clamp actuated with a piezo manipulator. The gap was estimated by tracking the capacitance change between the two devices. In a follow-up study in 2004, DiMatteo *et al.* [90] developed devices to probe even smaller gaps using tubular spacers [Fig. 5(a) bottom right panel]. Because of their long lengths, these spacers could reduce the parasitic conduction to heat flow, while their compliance allowed dynamic variation of the gap. Relative enhancements in power output of four- to tenfold were reported for near-field operation as compared with far-field operation for different PV cell designs with emitter temperatures up to 850 °C. However, a systematic gap-dependent measurement of the power output and the TPV performance could not be performed in these studies. Next, a contactless experiment was attempted by Hanamura and Mori [89] in 2007 between a tungsten emitter and a GaSb PV cell [Fig. 5(b)]. The tungsten emitter was heated to a maximum temperature of about 727 °C using a CO_2 laser incident on the emitter's backside. They observed an increase in power output as the gap size was reduced from 1000 μm to around 10 μm, as expected based on the increasing view factor. Importantly, a near-field enhancement in power was observed at gaps <1 μm, even when the temperature of the emitter decreased.

The next advancement in NF TPV experiments was achieved in 2018 by Fiorino *et al.* [8] [Fig. 6(a)]. Using a custom-built nanopositioner, in combination with a specially fabricated emitter and a commercial (In, As)Sb-based photodiode, they were able to directly observe an approximate 40-fold enhancement in the electrical power output of the PV cell as the gap was reduced from the FF to the NF. In these experiments, the emitter could be heated by passing an electrical current through a thin-film Pt resistor integrated into the emitter [Fig. 6(a) top panel],
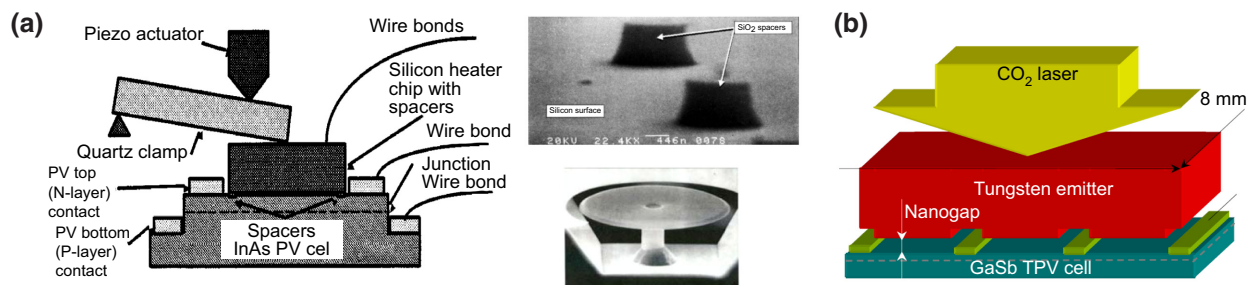

FIG. 5. Schematics of early experimental attempts for probing NF TPV energy conversion. (a) In a first attempt, a Si heater was pressed against an InAs photovoltaic cell via a quartz clamp. The silicon emitter was heated by passing current through an integrated resistor (left panel). To minimize the thermal contact between the hot Si emitter and the PV cell, special microfabricated spacers were used. A scanning electron micrograph of the spacers is shown in the top right panel. The bottom right panel shows microfabricated tubular spacers that further increased the thermal resistance to conductive heat transfer. Reproduced with permission from [76]. (b) In another experiment, a tungsten emitter was heated by shining a CO_2 laser on the backside and a multiaxis positioner was used to maintain a contactless microgap between the emitter and a GaSb-based PV cell. Reproduced with permission from [89].

and the emitter temperature was independently character-ized. As the gap size between the emitter at 655 K and the PV cell at 300 K was systematically reduced from 12 μm to about 60 nm, the power output was found to increase from 0.77 nW to 30.2 nW. Such large enhance-ments were also systematically observed at other emitter temperatures [Fig. 6(a) bottom panel]. The authors also developed a theoretical model to calculate the above-band-gap photon flux based on fluctuational electrodynamics and a scattering-matrix treatment of various layers in the system. The efficiency, defined as the ratio of the measured electrical power and the radiative heat transfer between the emitter and the PV cell, was estimated by theoreti-cally calculating the RHT, as a direct measurement was not possible. The efficiency of this system was low (about 0.02%) due to a mismatch in the areas of the emitter and the PV cell, the relatively low emitter temperatures, and the high sub-band-gap absorption in the thick substrate. Fol-lowed by this direct experimental demonstration, several groups explored NF TPV power enhancements in different systems.

For example, Inoue *et al*. [9] in 2019 developed a spacer-based approach to achieve small gaps between a 2-μm-thick Si emitter and a cold (In, Ga)As-based thin-film PV cell [Fig. 6(b) top panel]. They developed a fabrication technique where the Si emitter is physically bonded to the PV cell via a narrow beam. By comparing two devices with an average gap size of 1160 nm (far-field) and 140 nm (near-field), they reported a tenfold increase in the power output at the highest temperature of 1070 K [Fig. 6(b) bottom panel]. They estimated the efficiency of the system to be 0.98% at a power density of 120 W/m^2. In this work they employed a thin-film PV cell to min-imize the sub-band-gap absorption. The intermediate Si substrate shown in Fig. 6(b) (top panel) aids in minimizing the surface phonon polariton–mediated RHT flux.

In another work, Bhatt *et al*. [10] leveraged the advances in electrostatic nanoelectromechanical-system (NEMS) actuators to design an integrated NF TPV system based on a thin-film tungsten emitter and a Ge photodiode [Fig. 6(c) top panel]. The hot emitter was suspended via thin flexures and a SiO$_2$ separator, and was heated by pass-ing an electrical current. The gap between the emitter and the PV cell was reduced from the initial as-fabricated gap size of 500 nm to about 100 nm by electrostatically actu-ating the NEMS device. At the highest temperature of
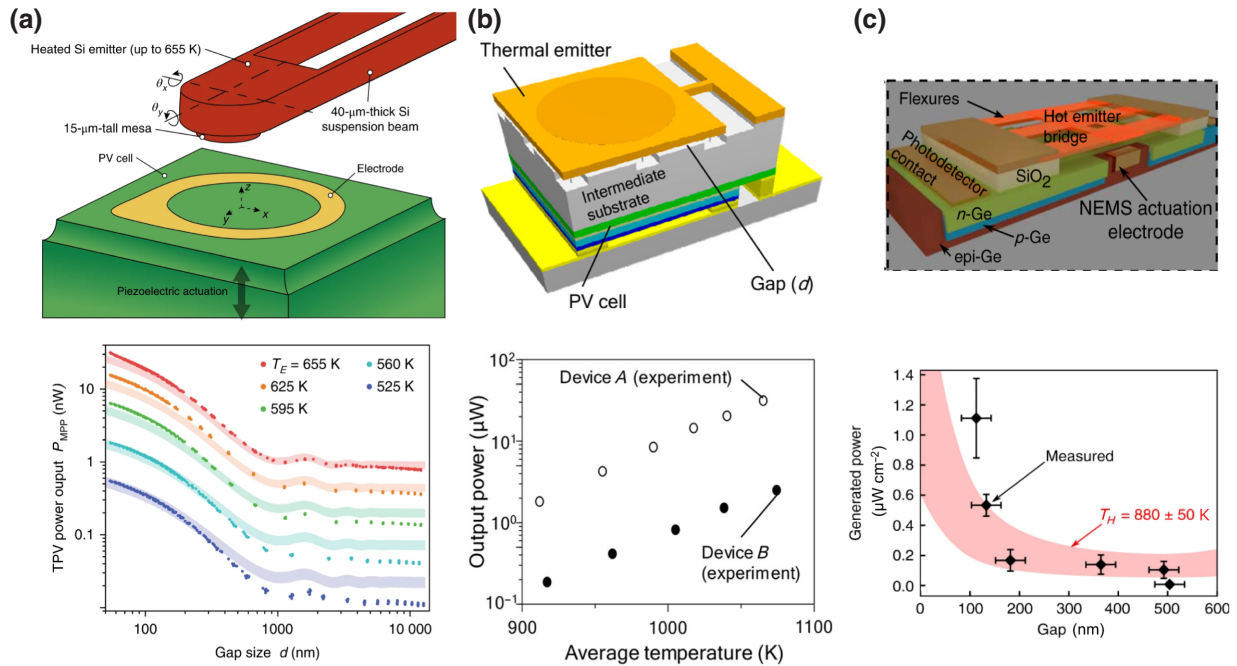

FIG. 6.   Summary of experimental work that quantitatively demonstrated power enhancements in NF TPV systems. (a) Top panel shows a microfabricated Si emitter heated via an integrated Pt resistor that was brought in proximity of a commercial PV cell via a custom-built nanopositioner. Bottom panel shows how the power output changes as the gap size reduced from tens of micrometers to tens of nanometers, at various emitter temperatures. Reproduced with permission from [8]. (b) Top panel shows a schematic of a single-chip NF TPV device where a Si heater was bonded to a (In, Ga)As-based PV cell via spacers to maintain the gap size. Bottom panel shows data from two different devices featuring different gap sizes (device *A*, average gap of 140 nm; device *B*, average gap of 1160 nm). Both devices indicated an enhancement in power output with increasing temperature consistent with theoretical expectations. Reproduced with permission from [9]. (c) Tungsten-coated Si-based emitter (orange region in top panel) in proximity of a Ge photodetector was heated by passing an electric current through the flexures and the gap size was varied by electrostatic actuation. An enhanced power output was seen as the gap size was reduced (bottom panel). Reproduced with permission from [10].

around 880 K, an 11-fold enhancement in power output was observed as the gap size reduced from 500 to 100 nm [Fig. 6(c) bottom panel]. They also measured a maximum power density of 0.01 W/m² at an efficiency of <0.01%. The relatively poor performance was attributed primarily to the relatively poor spectral overlap at an emitter temperature of 880 K and the Ge photodetector's low efficiency ($\eta_D \sim 3 \times 10^{-3}$%) that the authors attributed to defects in the growth stage. The three studies discussed here represent proof-of-principle experiments that experimentally confirm the potential of NF energy transport for TPV systems but feature low power density and efficiency. In the following, we discuss how recent work in the past five years, has tried to overcome these early shortcomings.

As discussed previously, the spectral overlap between the emitted radiation and the band gap of the PV cell plays an important role in determining the efficiency of the NF TPV system. On first consideration, low-band-gap PV cells seem particularly well suited for TPV systems operating with emitters at moderate temperatures, as such cells can potentially convert a large portion of the incident spectrum to electric power. However, typical low-band-gap materials (like InSb) suffer from relatively large dark currents at room temperature making them suboptimal for NF TPV applications. In IR detector applications they are normally (frequently) cooled to liquid-nitrogen temperature to reduce unacceptable dark currents. Recently, Lucchesi *et al.* [11] used a micrometer-sized InSb-based PV cell along with a graphite spherical emitter to probe a high-efficiency TPV system. They attached a 40-μm-diameter graphite sphere to a doped Si scanning thermal microscopy (SThM) probe, heated it to a temperature of 732 K, and brought it closer to an InSb cell that was cooled down to 77 K [Fig. 7(a) top panel]. In addition to measuring the NF power output as a function of gap size [Fig. 7(b) bottom panel], they monitored the resistance change of the SThM probe and indirectly estimated the near-field heat transfer flux. Based on averaging over several approaches, they observed a power output of around 7×10^3 W/m² at the smallest gap size with an estimated conversion efficiency of about 14% when the energetic cost for cooling is not considered.

In another recent study, Mittapally *et al.* [12] leveraged a nanopositioning system [8], doped Si emitters that could be heated to temperatures as high as 1300 K, and high-quality thin-film PV cells to study NF TPV energy conversion with uncooled cells [Fig. 7(b) top panel]. Instead of employing low-band-gap cells, they pursued an alternative approach that leveraged recent advances in III-V thin-film PV cell fabrication. Specifically, they employed a thin (In, Ga)As-based PV cell with a Au BSR [66]. This aids significantly in suppressing sub-band-gap absorption in the PV cell, thus reducing the heat transfer component while not affecting the above-band-gap energy transfer. The temperature of their emitter devices was measured

independently using a contact-based SThM technique. At the highest achieved temperature of 1270 K, they reported a power density of 5×10^3 W/m² at a calculated efficiency of 6.8% and a gap size of 100 nm. Their system allowed systematic exploration of the performance of NF TPV as a function of both gap size and temperature, revealing good agreement with their theoretical model [Fig. 7(b) middle and bottom panels]. This work also clearly demonstrates the potential of improving NF TPV performance to achieve increases in both power density and efficiency.

Finally, Inoue *et al.* [31] reported experiments where they employed a 20-μm-thick Si emitter and an (In, Ga)As PV cell. In this work they focused on improving the system efficiency, which they defined as the ratio of the measured power output to the input heating power. The emitter was designed with thin supporting beams that reduced thermal conduction losses [see Fig. 7(c) top panel]. This led to a large uncertainty in the gap sizes as noticed in their devices: 100–200-nm variations in the gap sizes reported over the 1 mm² area even at average gap sizes of 140 nm. Following this approach, the authors improved their system efficiency from 0.05% at 1065 K in their previous work [9] to 0.7% at 1192 K. Their best device (emitter at 1162 K) recorded a power output of 1.92×10^3 W/m² and a system efficiency of around 0.7% at a nominal gap size of 140 nm. This efficiency is still smaller than the estimated theoretical efficiency, which they attributed to the reduced reflectance of the Au BSR (from an ideal Au reflector with reflectivity $R_{Au} = 0.96$ to $R_{device} = 0.66$).

IV. ALTERNATIVE PHOTONIC HEAT ENGINES

A. Near-field thermoradiative power generation

An alternative concept for generating electricity, called TR generation, involves a PV cell that is in direct contact with a hot reservoir and radiatively interacting with a cold sink [Fig. 8(a)]. The principle of operation, while similar to that of a TPV cell, differs in how the current is generated. The TR cell generates power from a net flux of photons from the cell to the cold sink [Fig. 8(b)], which causes increased *e-h* pair recombination, resulting in separation of the quasi-Fermi-levels E_{Fh}, E_{Fe} and thus, creating a negative voltage bias across the PV cell under open circuit conditions [91]. Hence, for TR-based power generation, the *J-V* curve shifts to the second quadrant, in contrast with a TPV cell, which operates in the fourth quadrant [92] [Fig. 8(c)]. Like a PV cell in a TPV system, the PV cell in a TR system is also operated at a point where the power output is maximized. Thus, in a TR system, part of the heat supplied to keep the PV cell at a high temperature is converted to electrical power under reverse bias.

The possibility of developing a heat engine using a PV cell on the hot side of a photonic heat engine was first discussed by Byrnes *et al.* in 2014 [93]. In this work the
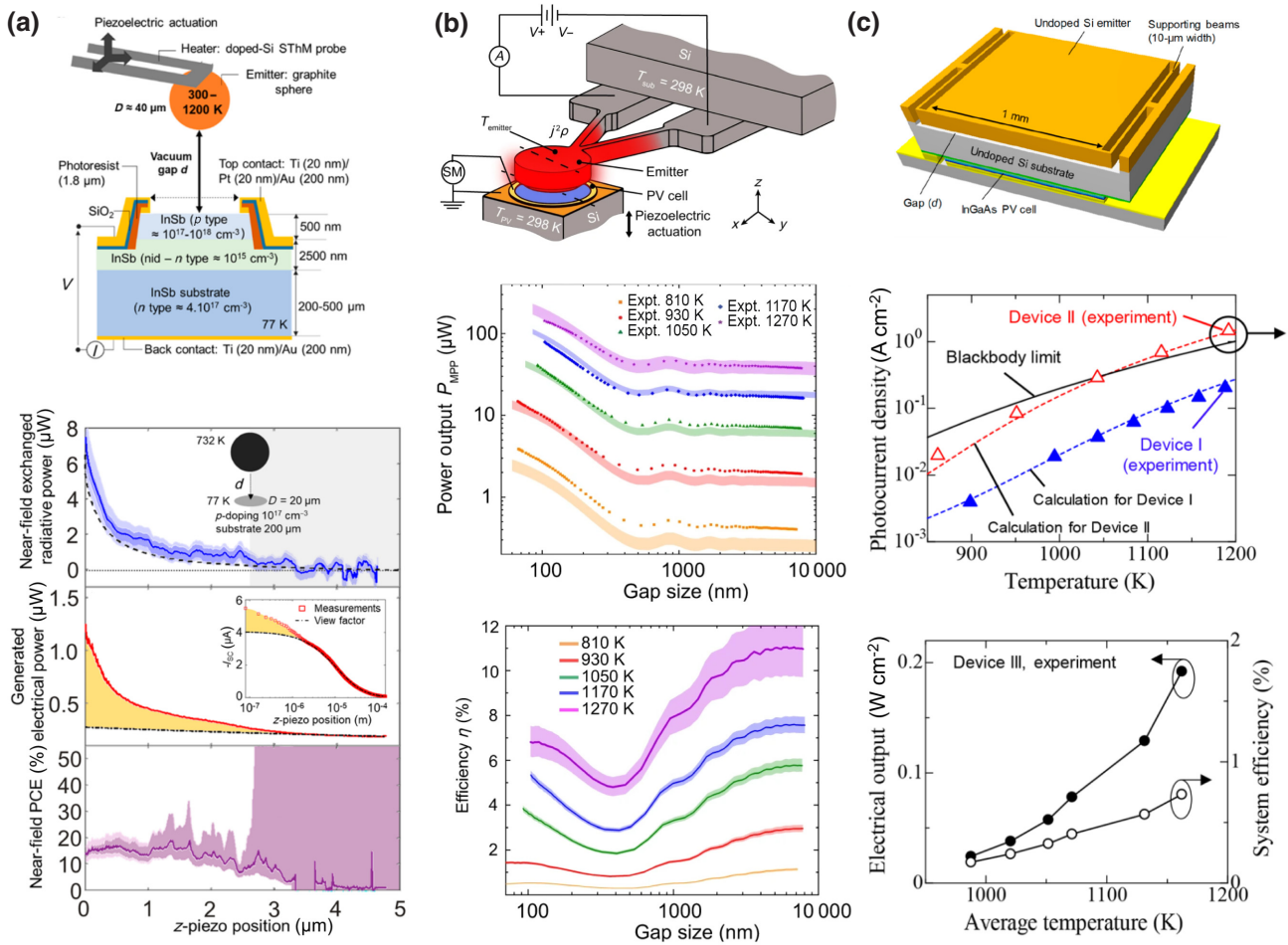
FIG. 7.   Data from recent experiments that demonstrated improved NF TPV performance. (a) Top panel shows the experimental configuration where a graphite sphere mounted on a SThM probe was heated to about 700 K and brought closer to an InSb PV cell cooled to 77 K. The measured electrical power output and the estimated radiative heat transfer as a function of gap size are shown in the bottom panels along with a calculated maximum efficiency of about 14%. Reproduced with permission from [11]. (b) Top panel shows a doped Si emitter heated by passing current through its beams and heated to around 1270 K. This was brought close to a thin-film (In, Ga)As PV cell and the gap systematically varied. The power output and the calculated efficiency as a function of gap size and temperatures are presented in the bottom panels. Reproduced with permission from [12]. (c) Top panel shows a schematic of an integrated NF TPV device using a thick Si emitter and an (In, Ga)As-based PV cell. Device I was operated in the far field, devices II and III in the near field. The bottom panels show the photocurrent density (for devices I and II) and the power output along with the system efficiency for device III [31]. Reproduced with permission from [31].

authors briefly mentioned the possibility of creating a heat engine involving a low-band-gap PV cell at room temperature that interacts with the cold reservoir at 3 K associated with outer space and generates power due to radiative recombination occurring more frequently than photogeneration as the incoming radiation is weak. However, the work of Byrnes *et al.* did not provide a quantitative analysis of TR generation involving PV cells, but rather analyzed heat engines involving rectennas (rectifying antennas that rectify electromagnetic waves to dc power output). The idea of creating PV-based TR devices was subsequently analyzed in detail by Strandberg [94], and the theoretical performance limits were evaluated by performing a Shockley-Queisser analysis on ideal PV cells. It was suggested that an ideal PV cell (E_g of 0.3 eV) maintained at 1000 K could deliver 1000 W/m^2 at an efficiency of 35.4% when placed in surroundings at a temperature of 300 K. Additional analysis presented in this work also suggested that larger-band-gap PV cells give higher peak efficiency, but less power. Strandberg's work [94] also suggested that, when choosing the band gap of PV cells for a TR power generation system, there exists a nontrivial trade-off between the efficiency and the power output of the system. Moreover, it was suggested that employing a BSR for the PV cell would improve the performance of TR cells as such a reflector prevents excitation of *e-h* pairs from the photons emitted by the underlying substrate.
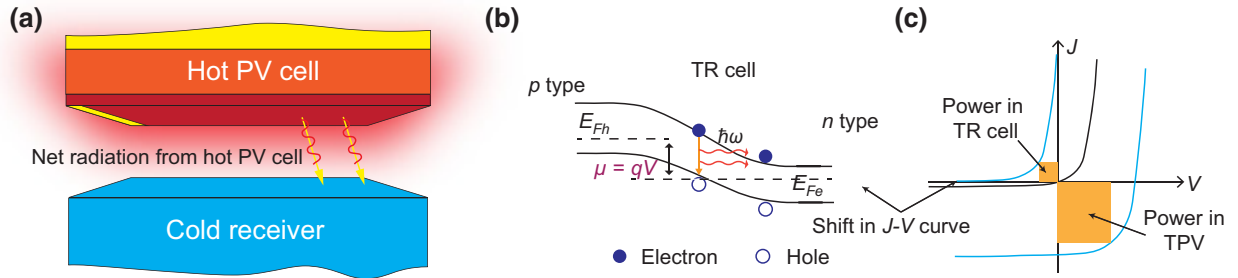
FIG. 8.   Working principle of a TR cell. (a) Heating a PV cell above the ambient temperature (i.e., the cold receiver) results in more radiative recombination than photogeneration. (b) Imbalance between recombination and photogeneration results in the separation of the quasi-Fermi-levels for holes and electrons. (c) This imbalance also results in shifting the *J-V* curve to the second quadrant reversing the signs of *J* and *V* when compared with a TPV system, but still results in a net positive power output. The orange shaded regions indicate the power that could be obtained in both the TR and TPV systems.

Experimental evidence of TR energy conversion in the far field was first obtained by Santhanam and Fan [95] in 2016, where an infrared photodiode [(Hg, Cd, Zn)Te, $E_g \sim 0.218$ eV at 300 K] facing a cold surface showed an increased photocurrent due to the TR effect, which they termed the negative illumination effect. They estimated the extractable power output by using the zero-bias resistance, as the *I-V* curves could not be obtained experimentally. More recently, the *I-V* curves were experimentally measured by Nielsen *et al*. [96] using (Hg, Cd)Te photodiodes, where they measured a power density of 2.26 mW/m^2 at an estimated radiative efficiency of 1.8%. Interestingly, the spectroscopic measurements on the PV cell show signatures of negative luminescence—a reduction in radiative recombination under negative bias [97,98]—which is essential for the TR operation. We note that the demonstrated systems [95,96] perform rather poorly due to the small temperature differential (<20 K in both measurements) between the PV cell and the cold receiver and due to significant nonradiative recombination losses.

The potential for achieving enhanced TR power extraction using NF effects was first discussed by Hsu *et al*. [99] in 2016, where, by means of entropy arguments, the authors concluded that the efficiency of TR systems can be improved by selectively emitting only low-frequency photons. From their calculations, the authors concluded that the surface phonon polariton modes in CaCO$_3$, typically occurring at around 0.186 eV, contribute to significant enhancements in energy flux when a CaCO$_3$ surface at 300 K is placed at nanometric separations from an InSb (at 500 K) PV cell with $E_g \sim 0.17$ eV. Specifically, they suggested that such a configuration could result in more than 3 orders of magnitude enhancement in power output along with an order of magnitude improvement in efficiency. Several other groups discussed performance improvements in NF TR systems via surface plasmon polariton–mediated energy transfer [100], by nanostructuring metallic surfaces [101], or by employing

hyperbolic metamaterials [102], which influence the spectral characteristics of energy transfer between the emitter and the PV cell.

The expected performance improvements in TR power generation by operating in the NF have not yet been experimentally demonstrated. Recent experimental advances in near-field radiative heat transfer, particularly in TPV systems, should enable experimental exploration of NF TR systems. We note that most theoretical studies considered ideal PV cells, where the radiative process through the interband transitions is the only mechanism for energy extraction. To better inform the design of practical systems, it appears essential for future studies to include temperature-dependent properties [88] of the semiconductor materials. Since low-band-gap PV cells have large dark currents, the optimal material for TR operation may in fact be a moderately large-band-gap PV cell (around 0.3–0.7 eV).

B. Near-field thermophotonic energy conversion

TPX systems involve an active light-emitting diode (LED) on the hot side—instead of a passive thermal emitter as in a TPV or a biased PV cell as in a TR cell—and a PV cell on the cold side. Briefly, TPX systems leverage the fact that electroluminescence from an LED has a higher radiation intensity (around the band gap of the LED) than a pure thermal emitter, as carrier recombination from injected charges leads to photogeneration. Thus, a hot LED can boost the radiative transfer compared with a passive thermal emitter at room temperature. Part of the power generated in the PV cell can then be used to run the LED, resulting in a net positive power output [103]. This approach to power generation is in principle possible because the LED extracts thermal energy from the hot body for producing high-intensity luminescence. This enhancement is closely related to electroluminescent
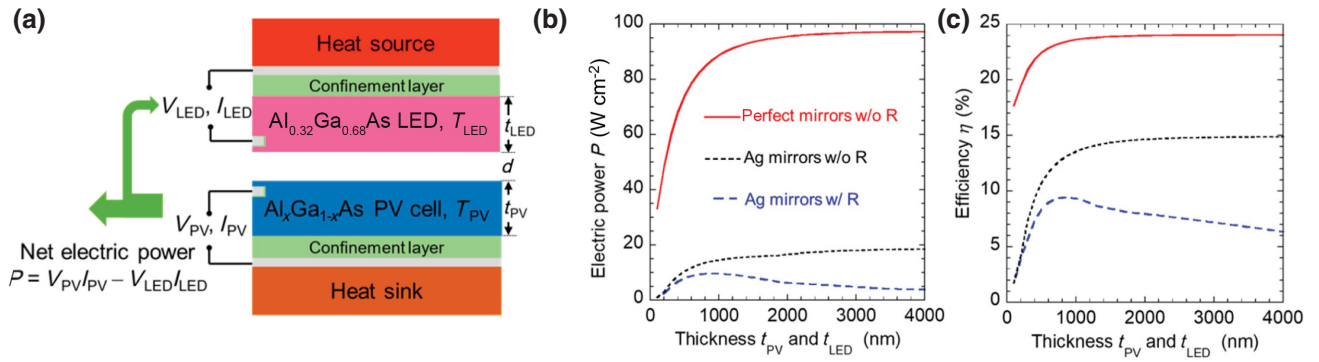
FIG. 9.   Operation and theoretical performance of a NF TPX system. (a) Schematic of a thermophotonic system consisting of $Al_{0.32}Ga_{0.68}As$ LED and a cold $Al_xGa_{1-x}As$ PV cell. The LED can be powered from the electricity generated by the system itself. Reproduced with permission from [105]. (b) and (c) Thickness dependence of electrical power and efficiency of the system shown in (a) with $T_{LED} = 600$ K and $T_{PV} = 300$ K. The solid red lines correspond to theoretical results obtained from a model for an ideal cell with perfect Ag mirrors and without nonradiative recombination R. The black dashed lines correspond to a model with realistic Ag dielectric function but without R. The blue dashed lines consider both the nonidealities and represent the more realistic case.

cooling in a LED [104], which demands a high external quantum efficiency and a low electrical resistance.

The performance of a TPX system is also expected to be enhanced by taking advantage of near-field effects, for example, by reducing the separation between the LED and the PV cell to nanoscale gaps. The potential of TPX enhancements in the near field was first studied by Zhao *et al.* [105] in 2018, where they simulated a system comprising an $Al_{0.32}Ga_{0.68}As$ LED at 600 K and an $Al_{0.155}Ga_{0.845}As$ PV cell at 300 K [Fig. 9(a)]. Considering thin-film optoelectronic structures, they suggested that it is possible to achieve power outputs of 9.6×10^4 W/m^2 at an efficiency of 9.8%, potentially outperforming thermoelectric generation. In their work, they also discussed the influence of the thickness of the structures [Figs. 9(b) and 9(c)] on the power output and efficiency. Specifically, they showed that the performance of the NF TPX system depends strongly on the reflectivity of the metal BSR and the nonradiative recombination rates in the PV cell and LED.

We note that in most theoretical studies of TPX systems it is assumed that the heated LED is powered by a battery, which is recharged by the power produced by the PV cell. The energy losses in this round trip could diminish the performance of NF TPX systems significantly. To address this, Zhao *et al.* [106] proposed the idea of a self-sustaining thermophotonic circuit, wherein a part of the energy generated by the PV cell is directly used to power the LED. They predicted that, by arranging a number of $N > 1$ LEDs connected in series and facing more than $M \geq 1$ PV cells in series, the system becomes self-sustaining when $N > M$. They further analyzed a system based on (Al, Ga)As emitters and PV cells—a system that is similar to the TPX device proposed in their previous work [105]—where the emitter is maintained at 600 K

and the cold sink is held at 300 K and predicted that a power output of around 1.1×10^6 W/m^2 is possible at a gap size of 10 nm. However, such large enhancements require LEDs possessing high external quantum efficiency ($>98\%$).

Another recent theoretical study by Yang *et al.* [107], involving a TPX system using a CdTe LED at 800 K and an InP PV cell at 300 K, suggested that it may be possible to obtain a power output of 1.91×10^4 W/m^2 at an efficiency of 48.2%. McSherry *et al.* [108] studied the influence of above-band-gap transmission bandwidth on the efficiency through simple models. These authors suggested that narrower transmission via surface phonon or plasmon polaritons may improve the efficiency of a NF TPX system. More recently, Legendre and Chapuis [109] performed a numerical analysis of a NF TPX system, where they coupled a NF RHT solver based on fluctuational electrodynamics with a simplified version of the one-dimensional drift-diffusion equations. In their modeling, they considered a GaAs-based PV cell at 300 K and a GaAs-based LED emitter at 600 K. They found that at a separation of 10 nm, this device had an overall efficiency of 1% when assuming an internal quantum efficiency of 0.9 and an electrical power output density of 1.1×10^4 W/m^2. This relatively low efficiency was attributed to the contribution of the below-band-gap photons that dominate the photon flux for this device.

The theoretical studies discussed here indicate that NF TPX can potentially perform better than NF TPV, particularly in the low temperature (around 400–900 K) range. We conclude by noting that, while theoretical and computational work suggests that NF TPX is an exciting new avenue for energy conversion, significant experimental efforts are needed to explore whether the computational predictions can indeed be realized.

V. REMARKS AND OUTLOOK

Near-field thermophotovoltaic systems offer new possibilities for directly converting heat to electricity with very high power output and efficiencies that are comparable to or even larger than efficiencies reported for FF TPV systems. The possibility of power enhancements beyond the blackbody limit enables TPV systems to potentially compete with thermoelectric systems. Advances in theoretical modeling of NF RHT have enabled detailed studies on NF TPV systems and can help pave the way for achieving large improvements in their performance. As discussed previously, recent experimental efforts have made progress towards achieving high-performance NF TPV systems. Further gains in efficiencies can potentially be obtained by engineering the emitters to selectively emit in the above-band-gap region along with minimized absorption in the sub-band-gap region. Additional insights into accomplishing this may be drawn from recent work, which has computationally explored the possibility of manipulating NF RHT and its spectra via tuning dielectric properties [110], developing thin-film and multilayer structures [111–113] as well as metasurfaces [114,115], and using nonreciprocal materials [58]. However, it is important to note that, while using insights from this work, it is also necessary to ensure that any strategies and materials used are compatible with the high temperatures at which emitters are operated.

Improving the PV cells to achieve a larger open-circuit voltage, smaller series resistance, and increased shunt resistance can also improve the performance of TPV systems. The open-circuit voltage can be enhanced by employing a hotter emitter, thus increasing the photocurrent. However, this increased current leads to additional energy loss through the series resistance, adversely impacting the total power generated. In fact, at high injection levels, it becomes critical to collect electrons and/or holes close to the source of generation. It has been suggested that the effect of the series resistance can be minimized by designing an electrical grid on top of the PV cell [116] or by designing a thermionic-enhanced NF TPV [29] as discussed previously. Another source of degradation in efficiency of (In, Ga)As-based PV cells is the large NF RHT in the sub-band-gap region brought about by surface phonon polaritons. This heat transfer could potentially be suppressed by depositing additional layers, e.g., amorphous Si, on top of the PV cell to minimize sub-band-gap NF RHT via surface phonon polaritons. While this strategy was attempted in Ref. [31], the full potential could not be realized, possibly due to the low reflectivity of their gold BSR. This limitation can potentially be addressed by incorporating an air-bridge reflector into the PV cell, similar to how it was implemented in earlier FF TPV systems [66]. In fact, such improvements are expected to enable efficiencies above 10%, but realizing these improvements experimentally remains challenging due to the practical difficulties in suspending a thin film and keeping it flat and clean.

Recent work in NF TPV systems [12,31] has leveraged advances in III-V PV cells to attain high performance. Further advances are likely possible by employing low-band-gap PV cells that utilize a large part of the spectrum to excite *e-h* pairs. For example, current efforts to reduce nonradiative recombination losses in low-band-gap PV cells [117] may enable future improvements to NF TPV performance, especially in the moderate temperature range (600–1000 K). Furthermore, we note that, to date, all NF TPV experiments have attained performance gains via tunneling of frustrated modes, which are expected to have an upper limit given by n^2 to the power enhancement as discussed previously. Enhancements larger than this are in principle possible by employing resonant modes, such as surface phonon polaritons [83] or plasmon polaritons [28,30,118,119]. However, experimental validation of these predictions has not been accomplished and future success in experimentally realizing these possibilities can significantly advance the performance of NF TPV systems.

We note that, in order to realize practical NF TPV systems, it will be necessary to address several electro-thermo-mechanical challenges. This is particularly daunting due to the limited availability of materials that are stable at high temperatures. Silicon is now well established to work at temperatures up to 1300 K [12,31] and performs as a suitable platform for exploring strategies to improve NF TPV performance. The NF performance of other high-temperature materials, such as rare earth oxides, that are thermodynamically stable [120], and photonic crystal structures based on tungsten or tantalum [121] should also be explored. In addition, another challenge that NF TPV systems may face is that of large attractive forces at nanoscale gaps, which arise either due to electrostatic forces or Casimir forces and can make it challenging to stably maintain small gap sizes. Recent advances in NF TPV and NF RHT studies present an opportunity to understand the physics of Casimir forces [122] (both equilibrium and nonequilibrium) in the plane-plane configuration and leverage these insights for creating future NF TPV technologies and for other applications in emerging NEMS devices.

A major bottleneck in realizing large-scale devices is the difficulty in maintaining a large temperature gradient between nanoscale separations with sufficient mechanical rigidity. These challenges can be tackled by including structures into the NF TPV system that provide mechanical support external to the emitter and the PV surfaces [9, 10,49,74,123,124], nanomanipulation systems with active control of the nanoscale gap [8,12,52,54], sparsely distributed micron beads [125–127], or lithographically integrated spacers [31,76,90,128–131]. While many studies employed these strategies to obtain nanoscale gaps, recent studies have also begun systematically exploring

the mechanical integrity of spacers [130–132] integrated into high-temperature energy conversion systems requiring micron to submicron gaps. Interestingly, Nicaise *et al.* [130] developed mechanically strong spacers by using silicon molds for achieving excellent thermal isolation between a hot emitter and a receiver but for micron-sized gaps. Further studies are needed for the systematic development of spacers for sub-100-nm-gap sized NF TPV structures. Practical NF TPV devices, if successfully developed, can have a strong positive impact on energy conversion technologies, especially when combined with improvements in thermal energy storage [133].

---

[1] D. Champier, Thermoelectric generators: A review of applications, Energy Convers. Manage. **140**, 167 (2017).

[2] A. Datas and A. Marti, Thermophotovoltaic energy in space applications: Review and future potential, Sol. Energy Mater. Sol. Cells **161**, 285 (2017).

[3] G. Xiao, G. H. Zheng, M. Qiu, Q. Li, D. S. Li, and M. J. Ni, Thermionic energy conversion for concentrating solar power, Appl. Energy **208**, 1318 (2017).

[4] J. He and T. M. Tritt, Advances in thermoelectric materials research: Looking back and moving forward, Science **357**, eaak9997 (2017).

[5] N. Jaziri, A. Boughamoura, J. Muller, B. Mezghani, F. Tounsi, and M. Ismail, A comprehensive review of thermoelectric generators: Technologies and common applications, Energy Rep. **6**, 264 (2020).

[6] F. Tohidi, S. G. Holagh, and A. Chitsaz, Thermoelectric generators: A comprehensive review of characteristics and applications, Appl. Therm. Eng. **201**, 117793 (2022).

[7] M. H. Elsheikh, D. A. Shnawah, M. F. M. Sabri, S. B. M. Said, M. H. Hassan, M. B. A. Bashir, and M. Mohamad, A review on thermoelectric renewable energy: Principle parameters that affect their performance, Renewable Sustainable Energy Rev. **30**, 337 (2014).

[8] A. Fiorino, L. Zhu, D. Thompson, R. Mittapally, P. Reddy, and E. Meyhofer, Nanogap near-field thermophotovoltaics, Nat. Nanotechnol. **13**, 806 (2018).

[9] T. Inoue, T. Koyama, D. D. Kang, K. Ikeda, T. Asano, and S. Noda, One-chip near-field thermophotovoltaic device integrating a thin-film thermal emitter and photovoltaic cell, Nano Lett. **19**, 3948 (2019).

[10] G. R. Bhatt, B. Zhao, S. Roberts, I. Datta, A. Mohanty, T. Lin, J. M. Hartmann, R. St-Gelais, S. Fan, and M. Lipson, Integrated near-field thermo-photovoltaics for heat recycling, Nat. Commun. **11**, 2545 (2020).

[11] C. Lucchesi, D. Cakiroglu, J. P. Perez, T. Taliercio, E. Tournie, P. O. Chapuis, and R. Vaillon, Near-field thermophotovoltaic conversion with high electrical power density and cell efficiency above 14%, Nano Lett. **21**, 4524 (2021).

[12] R. Mittapally, B. Lee, L. Zhu, A. Reihani, J. W. Lim, D. Fan, S. R. Forrest, P. Reddy, and E. Meyhofer, Near-field thermophotovoltaics for efficient heat to electricity conversion at high power density, Nat. Commun. **12**, 4364 (2021).

[13] K. F. Chen, P. Santhanam, S. Sandhu, L. X. Zhu, and S. H. Fan, Heat-flux control and solid-state cooling by regulating chemical potential of photons in near-field electromagnetic heat transfer, Phys. Rev. B **91**, 134301 (2015).

[14] L. X. Zhu, A. Fiorino, D. Thompson, R. Mittapally, E. Meyhofer, and P. Reddy, Near-field photonic cooling through control of the chemical potential of photons, Nature **566**, 239 (2019).

[15] B. Guha, C. Otey, C. B. Poitras, S. H. Fan, and M. Lipson, Near-field radiative cooling of nanostructures, Nano Lett. **12**, 4546 (2012).

[16] P. Ben-Abdallah and S. A. Biehs, Near-Field Thermal Transistor, Phys. Rev. Lett. **112**, 044301 (2014).

[17] A. Fiorino, D. Thompson, L. X. Zhu, R. Mittapally, S. A. Biehs, O. Bezencenet, N. El-Bondry, S. Bansropun, P. Ben-Abdallah, E. Meyhofer, and P. Reddy, A thermal diode based on nanoscale thermal radiation, ACS Nano **12**, 5774 (2018).

[18] C. R. Otey, W. T. Lau, and S. H. Fan, Thermal Rectification through Vacuum, Phys. Rev. Lett. **104**, 154301 (2010).

[19] Y. De Wilde, F. Formanek, R. Carminati, B. Gralak, P. A. Lemoine, K. Joulain, J. P. Mulet, Y. Chen, and J. J. Greffet, Thermal radiation scanning tunnelling microscopy, Nature **444**, 740 (2006).

[20] A. Kittel, U. F. Wischnath, J. Welker, O. Huth, F. Ruting, and S. A. Biehs, Near-field thermal imaging of nanostructured surfaces, Appl. Phys. Lett. **93**, 193109 (2008).

[21] A. C. Jones, B. T. O'Callahan, H. U. Yang, and M. B. Raschke, The thermal near-field: Coherence, spectroscopy, heat-transfer, and optical forces, Prog. Surf. Sci. **88**, 349 (2013).

[22] W. A. Challener, C. B. Peng, A. V. Itagi, D. Karns, W. Peng, Y. Y. Peng, X. M. Yang, X. B. Zhu, N. J. Gokemeijer, Y. T. Hsia, G. Ju, R. E. Rottmayer, M. A. Seigler, and E. C. Gage, Heat-assisted magnetic recording by a near-field transducer with efficient optical energy transfer, Nat. Photonics **3**, 220 (2009).

[23] F. P. Incropera and F. P. Incropera, *Fundamentals of heat and mass transfer*, 6th ed. (John Wiley, Hoboken, NJ, 2007).

[24] M. Laroche, R. Carminati, and J. J. Greffet, Near-field thermophotovoltaic energy conversion, J. Appl. Phys. **100**, 063704 (2006).

[25] K. Park, S. Basu, W. P. King, and Z. M. Zhang, Performance analysis of near-field thermophotovoltaic devices considering absorption distribution, J. Quant. Spectrosc. Radiat. Transfer **109**, 305 (2008).

[26] K. F. Chen, P. Santhanam, and S. H. Fan, Suppressing sub-bandgap phonon-polariton heat transfer in near-field thermophotovoltaic devices for waste heat recovery, Appl. Phys. Lett. **107**, 091106 (2015).

[27] J. K. Tong, W. C. Hsu, Y. Huang, S. V. Boriskina, and G. Chen, Thin-film 'thermal well' emitters and absorbers for high-efficiency thermophotovoltaics, Sci. Rep. **5**, 10661 (2015).

[28] B. Zhao, K. F. Chen, S. Buddhiraju, G. Bhatt, M. Lipson, and S. H. Fan, High-performance near-field thermophotovoltaics for waste heat recovery, Nano Energy **41**, 344 (2017).

[29] A. Datas and R. Vaillon, Thermionic-enhanced near-field thermophotovoltaics for medium-grade heat sources, Appl. Phys. Lett. **114**, 133501 (2019).

[30] G. T. Papadakis, S. Buddhiraju, Z. Zhao, B. Zhao, and S. Fan, Broadening near-field emission for performance enhancement in thermophotovoltaics, Nano Lett. **20**, 1654 (2020).

[31] T. Inoue, K. Ikeda, B. S. Song, T. Suzuki, K. Ishino, T. Asano, and S. Noda, Integrated near-field thermophotovoltaic device overcoming blackbody limit, ACS Photonics **8**, 2466 (2021).

[32] M. Planck, The theory of heat radiation, 2nd ed. (P. Blakiston's Son & Co., Philadelphia, PA) (1914).

[33] E. Rousseau, A. Siria, G. Jourdan, S. Volz, F. Comin, J. Chevrier, and J. J. Greffet, Radiative heat transfer at the nanoscale, Nat. Photonics **3**, 514 (2009).

[34] S. Shen, A. Narayanaswamy, and G. Chen, Surface phonon polaritons mediated energy transfer between nanoscale gaps, Nano Lett. **9**, 2909 (2009).

[35] K. Kim, B. Song, V. Fernandez-Hurtado, W. Lee, W. H. Jeong, L. J. Cui, D. Thompson, J. Feist, M. T. H. Reid, F. J. Garcia-Vidal, J. C. Cuevas, E. Meyhofer, and P. Reddy, Radiative heat transfer in the extreme near field, Nature **528**, 387 (2015).

[36] B. Song, Y. Ganjeh, S. Sadat, D. Thompson, A. Fiorino, V. Fernandez-Hurtado, J. Feist, F. J. Garcia-Vidal, J. C. Cuevas, P. Reddy, and E. Meyhofer, Enhancement of near-field radiative heat transfer using polar dielectric thin films, Nat. Nanotechnol. **10**, 253 (2015).

[37] D. Thompson, L. X. Zhu, R. Mittapally, S. Sadat, Z. Xing, P. McArdle, M. M. Qazilbash, P. Reddy, and E. Meyhofer, Hundred-fold enhancement in far-field radiative heat transfer over the blackbody limit, Nature **561**, 216 (2018).

[38] V. Fernandez-Hurtado, A. I. Fernandez-Dominguez, J. Feist, F. J. Garcia-Vidal, and J. C. Cuevas, Super-Planckian far-field radiative heat transfer, Phys. Rev. B **97**, 045408 (2018).

[39] S. Rytov, Y. Kravtsov, and V. Tatarskii, *Principles of statistical radiophysics* Vol. 3 (Springer, Berlin, 1989).

[40] D. Polder and M. Van Hove, Theory of radiative heat transfer between closely spaced bodies, Phys. Rev. B **4**, 3303 (1971).

[41] H. B. Callen and T. A. Welton, Irreversibility and Generalized Noise, Phys. Rev. **83**, 34 (1951).

[42] R. Kubo, The fluctuation-dissipation theorem, Rep. Prog. Phys. **29**, 255 (1966).

[43] C. M. Hargreaves, Anomalous radiative transfer between closely-spaced bodies, Phys. Lett. **30A**, 491 (1969).

[44] G. A. Domoto, R. F. Boehm, and C. L. Tien, Experimental investigation of radiative transfer between metallic surfaces at cryogenic temperatures, J. Heat Transfer **92**, 412 (1970).

[45] A. Kittel, W. Muller-Hirsch, J. Parisi, S. A. Biehs, D. Reddig, and M. Holthaus, Near-Field Heat Transfer in a Scanning Thermal Microscope, Phys. Rev. Lett. **95**, 224301 (2005).

[46] A. Narayanaswamy, S. Shen, and G. Chen, Near-field radiative heat transfer between a sphere and a substrate, Phys. Rev. B **78**, 115303 (2008).

[47] R. St-Gelais, B. Guha, L. X. Zhu, S. H. Fan, and M. Lipson, Demonstration of strong near-field radiative heat transfer between integrated nanostructures, Nano Lett. **14**, 6971 (2014).

[48] M. Lim, S. S. Lee, and B. J. Lee, Near-field thermal radiation between doped silicon plates at nanoscale gaps, Phys. Rev. B **91**, 1 (2015).

[49] M. P. Bernardi, D. Milovich, and M. Francoeur, Radiative heat transfer exceeding the blackbody limit between macroscale planar surfaces separated by a nanosize vacuum gap, Nat. Commun. **7**, 12900 (2016).

[50] B. Song, D. Thompson, A. Fiorino, Y. Ganjeh, P. Reddy, and E. Meyhofer, Radiative heat conductances between dielectric and metallic parallel plates with nanoscale gaps, Nat. Nanotechnol. **11**, 509 (2016).

[51] A. Fiorino, D. Thompson, L. X. Zhu, B. Song, P. Reddy, and E. Meyhofer, Giant enhancement in radiative heat transfer in sub-30 nm gaps of plane parallel surfaces, Nano Lett. **18**, 3711 (2018).

[52] M. Ghashami, H. Y. Geng, T. Kim, N. Iacopino, S. K. Cho, and K. Park, Precision Measurement of Phonon-Polaritonic Near-Field Energy Transfer between Macroscale Planar Structures Under Large Thermal Gradients, Phys. Rev. Lett. **120**, 175901 (2018).

[53] J. DeSutter, L. Tang, and M. Francoeur, A near-field radiative heat transfer device, Nat. Nanotechnol. **14**, 751 (2019).

[54] H. Salihoglu, W. Nam, L. Traverso, M. Segovia, P. K. Venuthurumilli, W. Liu, Y. Wei, W. J. Li, and X. F. Xu, Near-field thermal radiation between two plates with sub-10 nm vacuum separation, Nano Lett. **20**, 6091 (2020).

[55] L. Rincon-Garcia, D. Thompson, R. Mittapally, N. Agrait, E. Meyhofer, and P. Reddy, Enhancement and Saturation of Near-Field Radiative Heat Transfer in Nanogaps between Metallic Surfaces, Phys. Rev. Lett. **129**, 145901 (2022).

[56] B. Song, A. Fiorino, E. Meyhofer, and P. Reddy, Near-field radiative thermal transport: From theory to experiment, AIP Adv. **5**, 053503 (2015).

[57] J. C. Cuevas and F. J. Garcia-Vidal, Radiative Heat Transfer, ACS Photonics **5**, 3896 (2018).

[58] S. A. Biehs, R. Messina, P. S. Venkataram, A. W. Rodriguez, J. C. Cuevas, and P. Ben-Abdallah, Near-field radiative heat transfer in many-body systems, Rev. Mod. Phys. **93**, 025009 (2021).

[59] B. D. Wedlock, in *Proceedings of the IEEE* (1963), Vol. 51, pp. 694.

[60] R. M. Swanson, in *Proceedings of the IEEE* (1979), Vol. 67, pp. 446.

[61] R. E. Nelson, A brief history of thermophotovoltaic development, Semicond. Sci. Technol. **18**, S141 (2003).

[62] C. J. Crowley, N. A. Elkouh, S. Murray, and D. L. Chubb, Thermophotovoltaic converter performance for radioisotope power systems, AIP Conf. Proc. **746**, 601 (2005).

[63] V. L. Teofilo, P. Choong, W. Chen, J. Chang, and Y. L. Tseng, in *proceedings of Space Technology and Applications International Forum (STAIF-06), AIP Conf. Proc.* (2006), pp. 813.

[64] B. Wernsman, R. R. Siergiej, S. D. Link, R. G. Mahorter, M. N. Palmisiano, R. J. Wehrer, R. W. Schultz, G. P.

Schmuck, R. L. Messham, S. Murray, C. S. Murray, F. Newman, D. Taylor, D. M. DePoy, and T. Rahmlow, Greater than 20% radiant heat conversion efficiency of a thermophotovoltaic radiator/module system using reflective spectral control, IEEE Trans. Electron Devices **51,** 512 (2004).

[65] Z. Omair, G. Scranton, L. M. Pazos-Outon, T. P. Xiao, M. A. Steiner, V. Ganapati, P. F. Peterson, J. Holzrichter, H. Atwater, and E. Yablonovitch, Ultraefficient thermophotovoltaic power conversion by band-edge spectral filtering, Proc. Natl. Acad. Sci. U. S. A. **116,** 15356 (2019).

[66] D. Fan, T. Burger, S. McSherry, B. Lee, A. Lenert, and S. R. Forrest, Near-perfect photon utilization in an air-bridge thermophotovoltaic cell, Nature **586,** 237 (2020).

[67] A. LaPotin, K. L. Schulte, M. A. Steiner, K. Buznitsky, C. C. Kelsall, D. J. Friedman, E. J. Tervo, R. M. France, M. R. Young, A. Rohskopf, S. Verma, E. N. Wang, and A. Henry, Thermophotovoltaic efficiency of 40%, Nature **604,** 287 (2022).

[68] S. Basu, Y. B. Chen, and Z. M. Zhang, Microscale radiation in thermophotovoltaic devices - A review, Int. J. Energy Res. **31,** 689 (2007).

[69] T. Burger, C. Sempere, B. Roy-Layinde, and A. Lenert, Present efficiencies and future opportunities in thermophotovoltaics, Joule **4,** 1660 (2020).

[70] E. J. Tervo, R. M. France, D. J. Friedman, M. K. Arulanandam, R. R. King, T. C. Narayan, C. Luciano, D. P. Nizamian, B. A. Johnson, and A. R. Young, Efficient and scalable GaInAs thermophotovoltaic devices, Joule **6,** 2566 (2022).

[71] E. López, I. Artacho, and A. Datas, Thermophotovoltaic conversion efficiency measurement at high view factors, Sol. Energy Mater. Sol. Cells **250,** 112069 (2023).

[72] J. Song, J. Han, M. Choi, and B. J. Lee, Modeling and experiments of near-field thermophotovoltaic conversion: A review, Sol. Energy Mater. Sol. Cells **238,** 111556 (2022).

[73] L. Tang, J. DeSutter, and M. Francoeur, Near-field radiative heat transfer between dissimilar materials mediated by coupled surface phonon- and plasmon-polaritons, ACS Photonics **7,** 1304 (2020).

[74] M. Lim, J. Song, S. S. Lee, and B. J. Lee, Tailoring near-field thermal radiation between metallo-dielectric multilayers using coupled surface plasmon polaritons, Nat. Commun. **9,** 4302 (2018).

[75] J. P. Mulet, K. Joulain, R. Carminati, and J. J. Greffet, Enhanced radiative heat transfer at nanometric distances, Microscale Thermophys. Eng. **6,** 209 (2002).

[76] R. S. DiMatteo, P. Greiff, S. L. Finberg, K. A. Young-Waithe, H. K. H. Choy, M. M. Masaki, and C. G. Fonstad, Enhanced photogeneration of carriers in a semiconductor via coupling across a nonisothermal nanoscale vacuum gap, Appl. Phys. Lett. **79,** 1894 (2001).

[77] G. T. Papadakis, M. Orenstein, E. Yablonovitch, and S. H. Fan, Thermodynamics of Light Management in Near-Field Thermophotovoltaics, Phys. Rev. Appl. **16,** 064063 (2021).

[78] A. Narayanaswamy and Y. Zheng, A Green's function formalism of energy and momentum transfer in fluctuational electrodynamics, J. Quant. Spectrosc. Radiat. Transfer **132,** 12 (2014).

[79] D. M. Whittaker and I. S. Culshaw, Scattering-matrix treatment of patterned multilayer photonic structures, Phys. Rev. B **60,** 2610 (1999).

[80] W. Shockley and H. J. Queisser, Detailed balance limit of efficiency of p–n junction solar cells, J. Appl. Phys. **32,** 510 (1961).

[81] J. L. Pan, H. K. H. Choy, and C. G. Fonstad, Very large radiative transfer over small distances from a black body for thermophotovoltaic applications, IEEE Trans. Electron Devices **47,** 241 (2000).

[82] M. D. Whale and E. G. Cravalho, Modeling and performance of microscale thermophotovoltaic energy conversion devices, IEEE Trans. Energy Convers. **17,** 130 (2002).

[83] A. Narayanaswamy and G. Chen, Surface modes for near field thermophotovoltaics, Appl. Phys. Lett. **82,** 3544 (2003).

[84] T. J. Bright, L. P. Wang, and Z. M. Zhang, Performance of near-field thermophotovoltaic cells enhanced with a backside reflector, J. Heat Transfer **136,** 062701 (2014).

[85] M. Francoeur, R. Vaillon, and M. P. Menguc, Thermal impacts on the performance of nanoscale-gap thermophotovoltaic power generators, IEEE Trans. Energy Convers. **26,** 686 (2011).

[86] A. Datas and R. Vaillon, Thermionic-enhanced near-field thermophotovoltaics, Nano Energy **61,** 10 (2019).

[87] A. Bellucci, M. Mastellone, V. Serpente, M. Girolami, S. Kaciulis, A. Mezzi, D. M. Trucchi, E. Antolin, J. Villa, P. G. Linares, A. Marti, and A. Datas, Photovoltaic anodes for enhanced thermionic energy conversion, ACS Energy Lett. **5,** 1364 (2020).

[88] P. Singh and N. M. Ravindra, Temperature dependence of solar cell performance-an analysis, Sol. Energy Mater. Sol. Cells **101,** 36 (2012).

[89] K. Hanamura and K. Mori, Nano-gap TPV generation of electricity through evanescent wave in near-field above emitter surface, AIP Conf. Proc. **890,** 291 (2007).

[90] R. DiMatteo, P. Greiff, D. Seltzer, D. Meulenberg, E. Brown, E. Carlen, K. Kaiser, S. Finberg, H. Nguyen, J. Azarkevich, P. Baldasaro, J. Beausang, L. Danielson, M. Dashiell, D. DePoy, H. Ehsani, W. Topper, K. Rahner, and R. Siergiej, Nano-gap TPV generation of electricity through evanescent wave in near-field above emitter surface, AIP Conf. Proc. 738, 42 (2004).

[91] T. Deppe and J. N. Munday, Nighttime photovoltaic cells: Electrical power generation by optically coupling with deep space, ACS Photonics **7,** 1 (2020).

[92] E. J. Tervo, W. A. Callahan, E. S. Toberer, M. A. Steiner, and A. J. Ferguson, Solar thermoradiative-photovoltaic energy conversion, Cell Rep. Phys. Sci. **1,** 100258 (2020).

[93] S. J. Byrnes, R. Blanchard, and F. Capasso, Harvesting renewable energy from Earth's mid-infrared emissions, Proc. Natl. Acad. Sci. U. S. A. **111,** 3927 (2014).

[94] R. Strandberg, Theoretical efficiency limits for thermoradiative energy conversion, J. Appl. Phys. **117,** 055105 (2015).

[95] P. Santhanam and S. H. Fan, Thermal-to-electrical energy conversion by diodes under negative illumination, Phys. Rev. B **93,** 161410 (2016).

[96] M. P. Nielsen, A. Pusch, M. H. Sazzad, P. M. Pearce, P. J. Reece, and N. J. Ekins-Daukes, Thermoradiative power conversion from HgCdTe photodiodes and their current-voltage characteristics, ACS Photonics **9,** 1535 (2022).

[97] P. Berdahl, Radiant refrigeration by semiconductor diodes, J. Appl. Phys. **58,** 1369 (1985).

[98] C. T. Elliott, Negative luminescence and its applications, Philos. Trans. R. Soc., A **359,** 567 (2001).

[99] W. C. Hsu, J. K. Tong, B. L. Liao, Y. Huang, S. V. Boriskina, and G. Chen, Entropic and near-field improvements of thermoradiative cells, Sci. Rep. **6,** 34837 (2016).

[100] C. W. Lin, B. N. Wang, K. H. Teo, and Z. M. Zhang, Near-field enhancement of thermoradiative devices, J. Appl. Phys. **122,** 143102 (2017).

[101] B. N. Wang, C. W. Lin, K. H. Teo, and Z. M. Zhang, Thermoradiative device enhanced by near-field coupled structures, J. Quant. Spectrosc. Radiat. Transfer **196,** 10 (2017).

[102] A. Ghanekar, Y. P. Tian, X. J. Liu, and Y. Zheng, Performance enhancement of near-field thermoradiative devices using hyperbolic metamaterials, J. Photonics Energy **9,** 1 (2019).

[103] N. P. Harder and M. A. Green, Thermophotonics, Semicond. Sci. Tech. **18,** S270 (2003).

[104] T. Sadi, I. Radevici, and J. Oksanen, Thermophotonic cooling with light-emitting diodes, Nat. Photonics **14,** 205 (2020).

[105] B. Zhao, P. Santhanam, K. F. Chen, S. Buddhiraju, and S. H. Fan, Near-field thermophotonic systems for low-grade waste-heat recovery, Nano Lett. **18,** 5224 (2018).

[106] B. Zhao, S. Buddhiraju, P. Santhanam, K. F. Chen, and S. H. Fan, Self-sustaining thermophotonic circuits, Proc. Natl. Acad. Sci. U. S. A. **116,** 11596 (2019).

[107] F. Yang, K. F. Chen, Y. T. Zhao, S. K. Kim, X. B. Luo, and R. Hu, Near-field thermophotonic system for power generation and electroluminescent refrigeration, Appl. Phys. Lett. **120,** 053902 (2022).

[108] S. McSherry, T. Burger, and A. Lenert, Effects of narrow-band transport on near-field and far-field thermophotonic conversion, J. Photonics Energy **9,** 1 (2019).

[109] J. Legendre and P. O. Chapuis, GaAs-based near-field thermophotonic devices: Approaching the idealized case with one-dimensional PN junctions, Sol. Energy Mater. Sol. Cells **238,** 111594 (2022).

[110] L. Zhang and O. D. Miller, Optimal materials for maximum large-area near-field radiative heat transfer, ACS Photonics **7,** 3116 (2020).

[111] M. Francoeur, M. P. Menguc, and R. Vaillon, Near-field radiative heat transfer enhancement via surface phonon polaritons coupling in thin films, Appl. Phys. Lett. **93,** 043109 (2008).

[112] P. Ben-Abdallah, K. Joulain, J. Drevillon, and G. Domingues, Near-field heat transfer mediated by surface wave hybridization between two films, J. Appl. Phys. **106,** 044306 (2009).

[113] H. Iizuka and S. Fan, Significant Enhancement of Near-Field Electromagnetic Heat Transfer in a Multilayer Structure through Multiple Surface-States Coupling, Phys. Rev. Lett. **120,** 063901 (2018).

[114] V. Fernandez-Hurtado, F. J. Garcia-Vidal, S. H. Fan, and J. C. Cuevas, Enhancing Near-Field Radiative Heat Transfer with Si-based Metasurfaces, Phys. Rev. Lett. **118,** 203901 (2017).

[115] X. L. Liu, R. Z. Zhang, and Z. M. Zhang, Near-field radiative heat transfer with doped-silicon nanostructured metamaterials, Int. J. Heat Mass Tran. **73,** 389 (2014).

[116] A. Karalis and J. D. Joannopoulos, Front-electrode design for efficient near-field thermophotovoltaics, Proc. SPIE 11081, 1108127 (2019).

[117] R. Q. Yang, W. X. Huang, and M. B. Santos, Narrow bandgap photovoltaic cells, Sol. Energy Mater. Sol. Cells **238,** 111636 (2022).

[118] M. Lim, J. Song, J. Kim, S. S. Lee, I. Lee, and B. J. Lee, Optimization of a near-field thermophotovoltaic system operating at low temperature and large vacuum gap, J. Quant. Spectrosc. Radiat. Transfer **210,** 35 (2018).

[119] M. Lim, S. Jin, S. S. Lee, and B. J. Lee, Graphene-assisted Si-InSb thermophotovoltaic system for low temperature applications, Opt. Express **23,** A240 (2015).

[120] G. Adachi and N. Imanaka, The binary rare earth oxides, Chem. Rev. **98,** 1479 (1998).

[121] V. Rinnerbauer, S. Ndao, Y. X. Yeng, W. R. Chan, J. J. Senkevich, J. D. Joannopoulos, M. Soljacic, and I. Celanovic, Recent developments in high-temperature photonic crystals for energy conversion, Energy Environ. Sci. **5,** 8815 (2012).

[122] T. Gong, M. R. Corrado, A. R. Mahbub, C. Shelden, and J. N. Munday, Recent progress in engineering the Casimir effect - applications to nanophotonics, nanomechanics, and chemistry, Nanophotonics **10,** 523 (2021).

[123] J. H. Lee, I. Bargatin, B. K. Vancil, T. O. Gwinn, R. Maboudian, N. A. Melosh, and R. T. Howe, Microfabricated thermally isolated low work-function emitter, J. Microelectromech. Syst. **23,** 1182 (2014).

[124] D. B. King, J. R. Luke, and K. R. Zavadil, in *Space Technology and Applications International Forum-2001* (2001), Vol. 552, pp. 1152.

[125] K. A. Littau, K. Sahasrabuddhe, D. Barfield, H. Y. Yuan, Z. X. Shen, R. T. Howe, and N. A. Melosh, Microbead-separated thermionic energy converter with enhanced emission current, Phys. Chem. Chem. Phys. **15,** 14442 (2013).

[126] K. Ito, K. Nishikawa, A. Miura, H. Toshiyoshi, and H. Iizuka, Dynamic modulation of radiative heat transfer beyond the blackbody limit, Nano Lett. **17,** 4347 (2017).

[127] S. Lang, G. Sharma, S. Molesky, P. U. Kranzien, T. Jalas, Z. Jacob, A. Y. Petrov, and M. Eich, Dynamic measurement of near-field radiative heat transfer, Sci. Rep. **7,** 1 (2017).

[128] J. I. Watjen, B. Zhao, and Z. M. M. Zhang, Near-field radiative heat transfer between doped-Si parallel plates

separated by a spacing down to 200 nm, Appl. Phys. Lett. **109**, 203112 (2016).

[129] K. Ito, A. Miura, H. Iizuka, and H. Toshiyoshi, Parallel-plate submicron gap formed by micromachined low-density pillars for near-field radiative heat transfer, Appl. Phys. Lett. **106**, 083504 (2015).

[130] S. M. Nicaise, C. Lin, M. Azadi, T. Bozorg-Grayeli, P. Adebayo-Ige, D. E. Lilley, Y. Pfitzer, W. Cha, K. Van Houten, N. A. Melosh, R. T. Howe, J. W. Schwede, and I. Bargatin, Micron-gap spacers with ultra-high thermal resistance and mechanical robustness for direct energy conversion, Microsyst. Nanoeng. **5**, 31 (2019).

[131] A. Bellucci, G. Sabbatella, M. Girolami, M. Mastellone, V. Serpente, A. Mezzi, S. Kaciulis, B. Paci, A. Generosi, R. Polini, A. Vitulano, I. Vivaldi, M. Antonelli, and D. M. Trucchi, Dielectric micro- and sub-micrometric spacers for high-temperature energy converters, Energy Technol. **9**, 2000788 (2021).

[132] M. F. Campbell, T. J. Celenza, F. Schmitt, J. W. Schwede, and I. Bargatin, Progress toward high power output in thermionic energy converters, Adv. Sci. **8**, 2003812 (2021).

[133] A. Henry, R. Prasher, and A. Majumdar, Five thermal energy grand challenges for decarbonization, Nat. Energy **5**, 635 (2020).